NASA CR-144924
ASRL TR 180-1

FURTHER STUDIES OF STALL FLUTTER AND NONLINEAR DIVERGENCE OF TWO-DIMENSIONAL WINGS

John Dugundji
Inderjit Chopra

Aeroelastic and Structures Research Laobratory
Department of Aeronautics and Astronautics
Massachusetts Institute of Technology
Cambridge, Massachusetts 02139

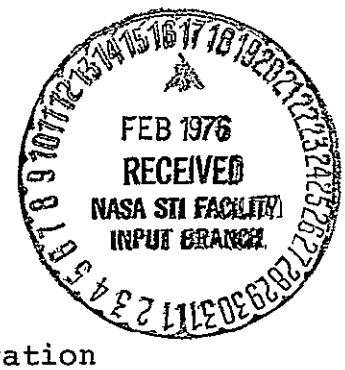

Prepared for

Langley Research Center
National Aeronautics and Space Administration
Hampton, Virginia 23665

Final Report, covering the period June 1974-August 1975
NASA Grant No. NSG 1051
Principal Investigator - J. Dugundji

N.O.P.O.

1. Report No.	2. Government Accession No.	3. Recipient's Catalog No.
NASA CR-144924		

4. Title and Subtitle	5. Report Date
FURTHER STUDIES OF STALL FLUTTER AND NONLINEAR DIVERGENCE OF TWO-DIMENSIONAL WINGS	6. Performing Organization Code

7. Author(s)	8. Performing Organization Report No.
John Dugundji and Inderjit Chopra	ASRL TR 180-1

9. Performing Organization Name and Address	10. Work Unit No.
Massachusetts Institute of Technology Aeroelastic and Structures Research Laboratory Cambridge, Massachusetts 02139	11. Contract or Grant No. NASA Grant NSG 1051

12. Sponsoring Agency Name and Address	13. Type of Report and Period Covered
National Aeronautics and Space Administration Washington, D.C. 20546	Final Report, Covering period, June 1974-Aug. 1975
	14. Sponsoring Agency Code

15. Supplementary Notes

Technical Officer: Wilmer H. Reed III, Structures & Dynamics Div., NASA Langley Research Center, Hampton, Virginia
Principal Investigator: John Dugundji

16. Abstract

An experimental investigation is made of the purely torsional stall flutter of a two-dimensional wing pivoted about the midchord, and also of the bending-torsion stall flutter of a two-dimensional wing pivoted about the quarterchord. For the purely torsional flutter case, large amplitude limit cycles ranging from ± 11 to ± 160 degrees were observed. Nondimensional harmonic coefficients were extracted from the free transient vibration tests for amplitudes up to 80 degrees. Reasonable nondimensional correlation was obtained for several wing configurations. For the bending-torsion flutter case, large amplitude coupled limit cycles were observed with torsional amplitudes as large as ± 40 degrees. The torsion amplitudes first increased, then decreased with increasing velocity. Additionally, a small amplitude, predominantly torsional flutter was observed when the static equilibrium angle was near the stall angle. The general trends found here might be of interest in related studies of wing stall flutter.

17. Key Words (Suggested by Author(s))	18 Distribution Statement
Stall Flutter Nonlinear Aeroelasticity Wing Divergence Bending-Torsion Flutter	Unclassified, Unlimited

19. Security Classif. (of this report)	20 Security Classif. (of this page)	21. No. of Pages	22. Price*
Unclassified	Unclassified	85	$4.75

* For sale by the National Technical Information Service, Springfield, Virginia 22161

ACKNOWLEDGEMENTS

The authors are indebted to Mr. Frank Durgin of the M.I.T. Wright Brothers Wind Tunnel, who originally conceived some of the flutter test mechanisms described here, and to Messrs. A. Shaw, J. Barley, and F. Merlis for their help with installing the instrumentation.

This work was sponsored by the National Aeronautics and Space Administration, Langley Research Center, Hampton, Virginia, under NASA Grant No. NSG 1051, "Nonlinear Aeroelasticity Research". The NASA Technical Officer for this grant was Mr. Wilmer H. Reed, III, NASA Langley Research Center, Hampton, Virginia.

SUMMARY

An experimental investigation is made of the purely torsional stall flutter of a two-dimensional wing pivoted about the midchord, and also of the bending-torsion stall flutter of a two-dimensional wing pivoted about the quarterchord. For the purely torsional flutter case, large amplitude limit cycles ranging from $\pm$ 11 to $\pm$ 160 degrees were observed. Nondimensional harmonic coefficients were extracted from the free transient vibration tests for amplitudes up to 80 degrees. Reasonable nondimensional correlation was obtained for several wing configurations. For the bending-torsion flutter case, large amplitude coupled limit cycles were observed with torsional amplitudes as large as $\pm$ 40 degrees. The torsion amplitudes first increased, then decreased with increasing velocity. Additionally, a small amplitude, predominantly torsional flutter was observed when the static equilibrium angle was near the stall angle. The general trends found here might be of interest in related studies of wing stall flutter.

CONTENTS

NOMENCLATURE

A	Amplitude of oscillation
a	Nondimensional location of elastic axis
b	Semichord = $c/2$
$C(k)$	Theodorsen function
C_L	Lift coefficient = $L/\frac{1}{2}\rho V^2 S$
C_{LI}, C_{LR}, C_{LO}	Harmonic lift coefficients
C_M	Moment coefficient = $M/\frac{1}{2}\rho V^2 S c$
C_{MI}, C_{MR}, C_{MO}	Harmonic moment coefficients
c	Chord
F	Real part of Theodorsen function
G	Imaginary part of Theodorsen function
g	Gravity
g	Structural damping
h	Bending displacement (positive up)
h_c	Bending displacement centershift
I	Moment of inertia of wing about pivot
I_V	Virtual aerodynamic moment of inertia
I_T	Total moment of inertia = $I + I_V$
i	$\sqrt{-1}$
k	Reduced frequency = $\omega b/V$
k_T	Torsional spring rate
k_h	Bending spring rate
k_α	Torsional spring rate including gravity effects
L	Lift
ℓ	Span of wing
M	Moment
M_{aero}	Aerodynamic moment
M_S	Spring moment

m	mass of wing
m_0, m_1, m_2	Aerodynamic moments defined by Eq. (12)
r_α	Nondimensional radius of gyration = $\sqrt{I/mb^2}$
S	Wing area
S_α	Static mass unbalance of wing
t	Time
V	Velocity of flow
W_F	Work due to friction
x_α	Nondimensional location of center of gravity = S_α/mb^2
α	Angle of attack
α_c	Centershift in angle of attack
α_i	Angle of attack for no spring moment
α_o	Initial angle of attack
α_s	Static equilibrium angle
$\Delta\alpha$	Incremental angle
ζ_T, ζ_F	Critical damping ratios (total and friction, respectively)
ζ_h, ζ_α	Critical damping ratios for bending and torsion motions
μ	Inertia density ratio = $4I/\rho Sc^3$
$\tilde{\mu}$	Mass density ratio = $m/\pi\rho b^2 \ell$
ρ	Air density
ω	Frequency of oscillation
ω_N	Natural frequency
ω_h, ω_α	Natural frequencies for bending and torsion

METRIC CONVERSIONS

1 cm	= .394 in
1 m	= 3.28 ft
1 m/sec	= 3.28 ft/sec
1 kg	= .0685 slugs
1 kg-m	= .225 slug-ft
1 $kg\text{-}m^2$	= .738 $slug\text{-}ft^2$
1 kg/m^3	= .001942 $slugs/ft^3$
1 N	= .225 lbf
1 N-m	= .738 lbf-ft
1 N/m	= .0685 lbf/ft
g = 9.82 m/sec^2	= 32.2 ft/sec^2

SECTION 1

INTRODUCTION

The present investigation attempts to explore the basic nonlinear flutter behavior of two-dimensional wings. There is much information, both theoretical and experimental, on linear flutter behavior, i.e., the onset of small amplitude, self-excited flutter. Much less is known, however, about the subsequent nonlinear behavior of the large amplitude flutter motions. For example, such a basic problem as predicting the steady-state amplitude of an actual wing flutter oscillation (assuming the wing is flexible enough so it doesn't break) is presently an extremely difficult task to do. At these large amplitudes of motion, aerodynamic stalling occurs and alleviates the aerodynamic forces. Further, because of the nonlinear aerodynamic forces, a wing that may be stable to small disturbances, might go into a large amplitude flutter oscillation, if given a large enough disturbance. Also, structural nonlinearities may be present which can affect the amplitude of the motion. Such considerations of large amplitude flutter (stall flutter) may play important roles in turbomachinery, helicopters, flexible wing aircraft, and building structures.

In a previous report involving one of the present authors, an experimental investigation was made of the purely torsional stall flutter and nonlinear divergence of a two-dimensional flat plate wing, pivoted about the midchord. See Dugundji and Aravamudan[1]. The present report continues that work by investigating further variations of the basic wing there and attempting to correlate the results nondimensionally. Also, the present report begins an investigation into the large amplitude, bending-torsion stall flutter behavior of a wing section pivoted about the quarterchord.

There have been many investigations of stall flutter in the past. The early work of Victory[2], Bratt and Wight[3], Halfman, Johnson, and Haley[4], Rainey[5,6], to mention a few names, has been

supplemented by more recent work on the subject (see for example, Refs. 7 through 15). Typical discussions of stall flutter applications to turbomachinery are given by Carta[16], to helicopters are given by Crimi[17], and to the space shuttle is given by Reed[18]. It is hoped the present report will contribute some additional knowledge to the behavior of wings oscillating at large amplitudes.

SECTION 2

TORSIONAL STALL FLUTTER OF A FLAT PLATE WING

2.1 Experiment

The experimental set-up for purely torsional stall flutter is shown in Fig. 1. A small wind tunnel with a 38.1-cm. x 5.7-cm. test section was used. One side wall of the test section was made of plexiglas for ease in viewing the test model behavior. The other side wall had an easily removable wood panel, 38.1-cm. x 38.1 cm. square, to which the test model and its supporting assembly were attached. The velocity of the wind tunnel could be adjusted continuously from 0 to 17 m/sec.

The two-dimensional flat plate wing was .64-cm. thick x 10.16-cm. chord, was pivoted about the midchord, and had a rounded leading edge and a square trailing edge. The wing was restrained by an .074-cm. diameter steel wire acting in torsion, which provided a linear torsional spring over very large angles. A low friction potentiometer measured the angular position of the wing, while a strain gage at the attachment block measured torsional moment. Also, angle lines were drawn every 5 degrees on the inside wall of the tunnel for visual observation of the angular position. The initial angle of attack could be varied through 360 degrees by rotating the entire wing support assembly.

Further details of the experimental set-up are given in Ref. 1. The overall test apparatus seemed to provide a relatively simple, low friction, linear torsional spring device to investigate large amplitude stall flutter. The nonlinearity entered here primarily through the aerodynamics, and no complicating structural nonlinearities were present.

In Ref. 1, the above set-up was used to take measurements of static moments, static divergence positions, flutter amplitudes, centershifts, frequencies, and decay-growth rates for a basic flat plate wing configuration. From these, nondimensional harmonic coefficients, $C_M = C_{MR} + i\, C_{MI}$, were deduced for the flat plate at an initial angle of attack $\alpha_o = 0^o$.

In the present report, the runs on the basic wing configuration were extended to other initial angles $\alpha_o = 5^o, 10^o, 15^o$, and the corresponding harmonic coefficients C_{MR}, C_{MI} and steady coefficient C_{MO} were deduced. Additionally, runs were made on the wing with a large added moment of inertia which decreased the torsional frequency from 8.2 Hz to 4.25 Hz. Also, runs were made on the wing with a heavier torsional spring (.091-cm. diameter) which increased the torsional frequency from 8.2 Hz to 12.0 Hz. Finally, the effect of nose bluntness was explored by pivoting the wing 180 degrees so that the square section end became the leading edge and the rounded end became the trailing edge.

The actual procedures for carrying out the above test runs were the same as those described in Ref. 1, and are discussed in more detail there. However, it should be mentioned again here, that, because of considerable blockage of the wind tunnel at high angles of attack, the velocity for any of the test runs was defined to be the velocity registered by the tunnel manometer when the wing section was brought to zero angle of attack manually and the variac power setting for the wind tunnel motor was not changed.

Figure 2 shows the measured static aerodynamic moment characteristics for the flat plate. These were obtained by replacing the basic .074-cm. diameter torsional spring wire by a much thicker .318-cm. diameter wire to prevent appreciable elastic twist, and then using the strain gage at the attachment to record the torsional moment. The measurements indicate a linear range from -9 to +8 degrees and a stalled region thereafter.

The static divergence characteristics of the flat plate are shown in Figs. 3a, b, c for the basic wing case, (.074-cm. torsional spring), increased inertia case, and increased spring case (.091-cm. torsional spring). These were obtained by giving the wing a specified initial angle of attack α_o, and then varying the tunnel velocity in small increments from 0 to 13 m/sec. The

resulting static angles α_s were obtained visually by viewing the wing against the angle lines drawn on the inside wall of the tunnel. For some of the lower initial angles α_o, it was necessary to lightly hold the wing pivot from the outside to prevent self-excited flutter oscillations from building up around the static equilibrium position. The measurements show a sharp rise in the $\alpha_o=0$ curves in the neighborhood of 5.5 m/sec for the basic wing and increased inertia cases, and about 8.0 m/sec for the increased spring case. These sharp rises represent a static divergence phenomenon. However, the nonlinear characteristics of the aerodynamic moment keep the static equilibrium angles finite.

The torsional stall flutter characteristics of the flat plate wing were investigated by giving the wing a specified angle of attack α_o, and then varying the tunnel velocity in small increments from 0 to 13 m/sec, as for the static divergence tests. At a given velocity, the wing section was manually given various disturbance angles $\Delta\alpha$ from the equilibrium position, then let go, and the resulting transient potentiometer position signal was recorded. This gave much data for transiently analyzing the response. Also, the amount of disturbance $\Delta\alpha$ needed to cause the wing to go into a steady flutter limit cycle oscillation was noted as well as the oscillation amplitude, centershift, and oscillation frequency. Before and after each test run, a static calibration was taken for the angular position signal, and also a transient decay record from a 90 degree twist angle for the natural frequency and critical damping ratio at zero velocity.

Figure 4a shows the measured amplitudes of the stall flutter for the basic wing case. Some of these amplitudes reached $\pm$ 100 degrees at the higher velocities. The dotted lines indicate roughly the amount of disturbance $\Delta\alpha$ required to cause the stall flutter limit cycle. It can be seen that self-excitation occurs for initial angles α_o between 0 and 8 degrees. Thereafter, increasingly larger disturbances $\Delta\alpha$ are required as α_o increases. Apparently, above a certain critical velocity, stall flutter is initiated if the wing angle gets near the stall angle of about 10 degrees, either by sufficiently large disturbances $\Delta\alpha$ (for

high α_o) or by the natural divergence process (for low α_o). Also, the gradual change in the flutter amplitude curves from $\alpha_o=0^o$ to 15^o is apparent in Fig. 4a. In fact, for $\alpha_o=5^o$, two different amplitude flutter limit cycles can occur at $V \simeq 5.5$ m/sec depending on the initial disturbance $\Delta\alpha$. A short movie was made of several of these limit cycles for the basic wing case.

Figures 4b and 4c shown the corresponding flutter amplitudes for the increased inertia and increased spring case respectively. The increased spring curves are similar in shape to the basic wing case with the velocities for a given amplitude increased proportionally. The increased inertia curves have a somewhat different shape with more double limit cycles over the range $\alpha_o=5^o$ to 15^o, and the velocities for a given amplitude are decreased from the basic wing case.

The flutter oscillation frequency ω and the centershift α_c at flutter were also recorded and plotted for the three wing cases, but are not shown here. Generally, the flutter frequencies were slightly lower than the natural frequencies ω_N except at low flutter amplitudes $A < 50^o$, where they decreased somewhat. Similarly the centershifts were close to the initial angles α_o except at low amplitudes where they increased somewhat. Curves of flutter frequency and centershift for the basic wing case are shown in Ref. 1.

As mentioned previously, many transient responses were obtained in addition to the steady state flutter limit cycles. The amplitudes of these transient decays (or growths) were plotted versus cycles (effective time) on semi-log paper, and from the resulting slopes of these semi-log plots, the critical damping ratios ζ could be obtained as functions of amplitude A. Also, the frequency ω and center shift α_c were obtained as functions of amplitude A. Such plots of ζ, ω, α_c versus amplitude A are shown in Ref. 1 for the basic wing case. It should be mentioned that all transient responses were read carefully with a magnifying glass and the amplitudes, frequencies, and centershifts were subsequently

smoothed by a numerical averaging process.

To obtain the purely frictional damping for the basic wing, the increased inertia wing, and the increased spring wing cases, the transient decay records at zero velocity were repeated with the wings replaced by a small 3.18-cm. diameter steel disk having the same moment of inertia as the wing. These disk results presumably had negligible aerodynamic damping and hence were indicative of the friction in the bearings and potentiometer. Values of the friction damping ratios ζ_F for the three cases are given in Fig. 5. The critical damping ratios increase as the amplitude A decreases. This is indicative of Coulomb type damping. Also, the ζ_F for the increased spring seems somewhat lower than for the basic wing and increased inertia cases.

In the analysis of the transient response records at a given tunnel velocity, it is well to point out that obtaining the total damping ratio ζ_T as a function of amplitude was not always a precise procedure, and in some cases involved some judgment in reading the response traces. This arose from the presence of "overshoots" in some of the responses which had to be faired in reasonably. Examples of these are given in Ref. 1. Generally, the basic wing and increased inertia wing had fewer of these "overshoots" and the total damping results ζ_T were reasonably indicative of the actual behavior. The increased spring wing, however, had many of these "overshoots" and the transient response analysis was not done for this case. Only steady-state oscillation cases $\zeta_T=0$ were used here.

2.2 Theory and Discussion

The static aerodynamic characteristics of the flat plate wing about its midchord are expressed by the nondimensional coefficient C_M as,

$$C_M = \frac{M}{\frac{1}{2}\rho V^2 S c} \qquad (1)$$

For a two-dimensional flat plate in incompressible flow, the

theoretical moment curve slope in the linear (unstalled) region is

$$\frac{dC_M}{d\alpha} = \frac{\pi}{2} = 1.57 \qquad (2)$$

for the wing pivoted about the midchord. This theoretical value compares reasonably with the experimentally measured value of 1.39 per radian shown in Fig. 2. The somewhat lower value here is mainly due to the blunt trailing edge and associated viscosity effects which prevent the full theoretical lift-curve slope of 2π from being achieved.

The linear divergence speed for the wing can be found by considering static moment equilibrium about the midchord, namely,

$$\tfrac{1}{2}\rho V^2 S c C_M - k_T(\alpha - \alpha_o) = 0 \qquad (3)$$

where k_T is the torsional spring rate and α_o is the initial angle of attack. Setting $C_M = (dC_M/d\alpha)\alpha$ in Eq. (1), then solving for α, then noting when $\alpha \to \infty$, results in the linear divergence speed,

$$V_D = \sqrt{\frac{2k_T}{\rho S c \frac{dC_M}{d\alpha}}} \qquad (4)$$

The measured experimental values for the basic wing, the increased inertia wing, and the increased spring wing are given in Fig. 6. Placing these values into Eq. (4) gives calculated divergence speeds of 5.7 m/sec, 5.7 m/sec, and 8.3 m/sec respectively for the three cases. These linear divergence speeds are indicated in Figs. 3a, b, c by a small arrow and agree well with the sharp rise in the observed static angle α_s in that vicinity for the α_o=0 cases.

The actual static divergence characteristics of the flat plate wing are governed by the nonlinear C_M versus α curve shown in Fig. 2, rather than the linear relation, Eq. (2), which is valid only for α between -9 to +8 degrees. To obtain these

nonlinear static divergence characteristics, one rearranges Eq. (3) in the form,

$$C_M = \frac{2 k_T}{\rho V^2 S c} (\alpha - \alpha_o) \tag{5}$$

The left-hand side of Eq. (5) represents the C_M versus α curve of Fig. 2, while the right-hand side represents a straight line of slope $2k_T/\rho V^2 Sc$ which passes through the point $C_M=0$, $\alpha=\alpha_o$. A graphical solution of Eq. (5) is easily obtained by locating the intersection of the straight line with the C_M versus α curve. Note that for low velocities, there will be only one solution while for higher velocities there will be three (but the second solution is always statically unstable).

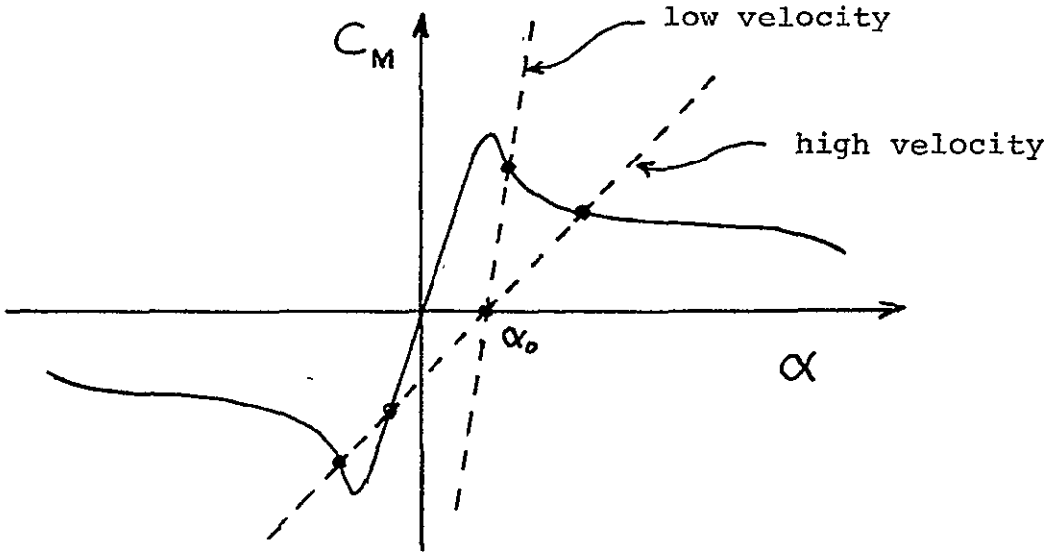

Graphical Solution of Eq. (5)

Figures 3a, b, c show the calculated static equilibrium angles as determined by this method for the three flat plate wing cases. Good agreement with experiment is found over the given range of initial angles α_o for all three wing cases. It is interesting to note that the nonlinear divergence phenomenon here resembles the nonlinear buckling of plates with varying amounts of initial imperfection.

The dynamic behavior of the wing torsional system with no aerodynamic forces present can be represented by the standard equation,

$$I\ddot{\alpha} + 2\zeta_F \omega_N \dot{\alpha} + k_T \alpha = 0 \tag{6}$$

where I is the moment of inertia about the midchord, $\omega_N = \sqrt{k_T/I}$ is the natural frequency of the wing, and ζ_F is the critical damping ratio due to the bearing and potentiometer friction. Experimental values of k_T, ω_N, and I for the basic wing, the increased inertia wing, and the increased spring wing are given in Fig. 6. In these k_T and ω_N were measured directly from static and free vibration tests while I was determined from these measured values of k_T and ω_N by using the relation, $I = k_T/\omega_N^2$. The amount of virtual inertia of air that would contribute to this value of I, can be estimated from two-dimensional aerodynamic theory (Ref. 19) as,

$$I_v = \frac{\pi \rho S c^3}{128} \tag{7}$$

This result is $I_V = .18 \times 10^{-6}$ kg-m^2 which would give a negligible contribution here. The friction critical damping ratios ζ_F for the three wing cases were measured from transient decay records as mentioned earlier, with the wing replaced by a solid disk of equivalent inertia. The results are given in Fig. 5 and are seen to be functions of oscillation amplitude A, thereby indicating nonlinear damping behavior. The qualitative form of this friction damping can be deduced roughly by considering the concept of "equivalent damping", Ref. 20, as follows.

For the bearing and potentiometer friction, the resisting moment M_F is apt to be predominantly a Coulomb friction-type moment of constant magnitude, i.e., $M_F = c_1$. Assuming harmonic motion, $\alpha = A \cos \omega t$, the work done over one cycle is,

$$W_F = 4 \int_0^{\pi/4} M_F \dot{\alpha} \, dt = 4 c_1 A \qquad (8)$$

For the usual viscous-type resisting moment $M_V = 2\zeta \omega_N I \dot{\alpha}$, the work done over one cycle is,

$$W_F = 4 \int_0^{\pi/4} M_V \dot{\alpha} \, dt = 2 \zeta \omega_N I \pi \omega A^2 \qquad (9)$$

Equating the work done for these two cases gives the equivalent critical damping ratio as,

$$\zeta_F = \frac{.636 \, c_1}{k_T A (\omega/\omega_N)} \qquad (10)$$

Since $\omega \sim \omega_N$ here, the ζ_F should vary inversely with amplitude A. Also, increasing the stiffness will lower the damping ratio ζ_F, whereas increasing the inertia will have no effect. All these trends are borne out by the experimental results given in Fig. 5. Of course, some viscous and other type dampings may also be

present in the actual friction which may modify the theoretical results somewhat, but Eq. (10) characterizes the predominant components here.

The stall flutter characteristics of the flat plate wing at a wind velocity V can be represented by the equation,

$$I\ddot{\alpha} + 2\zeta_F \omega_N I\dot{\alpha} + k_T(\alpha - \alpha_o) = M_{aero} \qquad (11)$$

where the aerodynamic moment is given by

$$M_{aero} = \tfrac{1}{2}\rho V^2 S c \left[m_o + m_1(\alpha - \alpha_c) + m_2 \frac{b\dot{\alpha}}{V}\right] - I_v\ddot{\alpha} \qquad (12)$$

In the above, ω_N represents the natural frequency without the air, b is the semichord, I_v is the aerodynamic virtual mass, while m_2, m_1, and m_0 specify the additional aerodynamic damping, spring, and constant moment, respectively, due to the wind velocity. The aerodynamic quantities m_2, m_1, and m_0 are nondimensional, and are assumed here to be functions of oscillation amplitude A, centershift α_c about which the oscillation takes place, and reduced frequency $\omega b/V$ (actually, the static m_0 term may be considered roughly independent of $\omega b/V$). One can then combine Eqs. (11) and (12) into the standard form,

$$\ddot{\alpha} + 2\zeta_T \omega \dot{\alpha} + \omega^2 \alpha = \omega^2 \alpha_c \qquad (13)$$

where ζ_T represents the total critical damping ratio, ω the natural frequency, and α_c the centershift, respectively, of the system response in the presence of the wind velocity. The quantities ζ_T, ω, α_c generally vary slowly during the response, and are assumed here to be functions of oscillation amplitude A.

From transient decay records of the wing at a given velocity V and initial angle of attack setting α_o, the critical damping

---

*Note, there is a slightly different definition of m_0 and m_1 here than was given in Ref. 1, because of the α_c term. Also, virtual mass is included here.

ratio ζ_T, frequency ω, and centershift α_c can be obtained as functions of amplitude A. Then from Eqs. (11), (12), (13), one can determine the aerodynamic quantities m_2, m_1, m_0 of Eq. (12) as,

$$m_2 = 4\mu \frac{\omega b}{V}\left[\zeta_F \frac{\omega_N}{\omega} - \zeta_T \frac{I_T}{I}\right] \tag{14}$$

$$m_1 = 2\mu \left(\frac{\omega b}{V}\right)^2\left[\left(\frac{\omega_N}{\omega}\right)^2 - \frac{I_T}{I}\right] \tag{15}$$

$$m_0 = 2\mu \left(\frac{\omega b}{V}\right)^2\left(\frac{\omega_N}{\omega}\right)^2\left[\alpha_c - \alpha_0\right] \tag{16}$$

where $\mu \equiv 4I/\rho Sc^3$ is an inertia density ratio parameter, while $I_T = I + I_V$ represents the total moment of inertia of the system. The virtual mass I_V can be either estimated from theory using Eq. (7), or can be deduced from natural frequency measurements at zero velocity with and without the fluid medium present. If air is the fluid medium (as here), then the tests must be done in air and in a vacuum; if water is the fluid medium, the tests can usually be done in water and in air.

The aerodynamic moment M_{aero} given by Eq. (12) can also be expressed in the standard harmonic coefficient form by assuming harmonic motion about some centershift α_c as,

$$\alpha(t) = \alpha_c + A e^{i\omega t} \tag{17}$$

and then writing,

$$M_{aero} = \tfrac{1}{2}\rho V^2 S c\left[C_{M0} + \left(C_{MR} + i\, C_{MI}\right)e^{i\omega t}\right] \tag{18}$$

Upon substitution of Eq. (17) into (12), comparing with Eq. (18) and using Eqs. (14), (15), (16), one can express the harmonic coefficients as

$$C_{MI} = m_2 A \frac{\omega b}{V} = 4\mu \left(\frac{\omega b}{V}\right)^2 A \left[\zeta_F \frac{\omega_N}{\omega} - \zeta_T \frac{I_T}{I}\right] \tag{19}$$

$$C_{MR} = m_1 A + \frac{8 I_v}{\rho S c^3}\left(\frac{\omega b}{V}\right)^2 A = \left(\frac{\omega b}{V}\right)^2 A \left\{2\mu\left[\left(\frac{\omega_N}{\omega}\right)^2 - \frac{I_T}{I}\right] + \frac{8 I_v}{\rho S c^3}\right\} \tag{20}$$

$$C_{MO} = m_o = 2\mu \left(\frac{\omega b}{V}\right)^2 \left(\frac{\omega_N}{\omega}\right)^2 (\alpha_c - \alpha_o) \tag{21}$$

As in Eqs. (11) and (12), the above harmonic moment coefficients are similarly functions of amplitude A, centershift α_c, and reduced frequency $\omega b/V$, while the static C_{MO} term may be considered roughly independent of $\omega b/V$. Note also that the nondimensional parameter $k_T/\rho V^2 Sc$ which appeared in the static divergence analysis Eq. (5), can be expressed alternatively as,

$$\frac{k_T}{\rho V^2 S c} = \mu \left(\frac{\omega b}{V}\right)^2 \left(\frac{\omega_N}{\omega}\right)^2 \tag{22}$$

Experimental values of k_T, ω_N, I and μ for the basic wing, the increased inertia wing, and the increased spring wing are given in Fig. 6. As mentioned previously, for these wing cases, the virtual mass contribution I_v estimated from Eq. (7) was found to be negligible. Hence in all previous Eqs. (12) to (21), one sets $I_v=0$ and $I_T/I=1$.

Figures 7a-d, 8a-d, 9a-e, show the experimental harmonic coefficients C_{MI}, C_{MR}, C_{MO}, respectively for $\alpha_c \approx 0^o$, 6^o, 11^o, 16^o and various values of amplitude A and reduced velocity, $V/\omega b$. These were obtained by applying Eqs. (19), (20), (21) with $I_v=0$, $I_T/I=1$ to the measured transient response values of ζ_T, ω, α_c for

the three wing cases. Reasonable agreement for the harmonic coefficients was generally obtained by the three different wing cases, thereby bearing out the basic nondimensionalization process. Looking at the C_{MI} curves, Figs. 7a-d, it seems that the larger amplitude A=40°, 60°, 80° curves do not change much in shape or magnitude in going from centershifts α_c=0° to α_c=16°, but the A=10° and 20° curves do change considerably. In particular, the A=10° curve is always stable (negative C_{MI}) for all V/ωb at $\alpha_c \simeq 0°$, but becomes unstable at a lower and lower V/ωb as α_c increases. The lowest instability (positive C_{MI}) generally sets in around V/bω ≃ 2, except for $\alpha_c \simeq 16°$ where it becomes a little less at the lower amplitudes. Looking at the C_{MR} curves Figs. 8a-d, it appears again that the larger amplitude A=40°, 60°, 80° curves do not change much in shape and magnitude but the lower amplitude A=10° and 20° curves give lower magnitudes as α_c increases. Looking at the C_{MO} curves Figs. 9a-e, it appears that despite the scatter, the C_{MO} coefficient correlates reasonably with α_c and A only. A previous attempt to correlate additionally with V/bω as for C_{MI} and C_{MR} gave a meaningless jumble.

The linear, two-dimensional theory solution for a flat plate oscillating in rotation about its midchord is given as (see Ref. 19),

$$M_{aero} = -\frac{\pi \rho b^4 \ell}{8}\ddot{\alpha} - \frac{\pi \rho b^3 V \ell}{2}\dot{\alpha} + \frac{1}{2}\rho V^2 b^2 \ell \, 2\pi C(k)\left[\alpha + \frac{1}{2}\frac{b\dot{\alpha}}{V}\right] \tag{23}$$

where ℓ is the span, k = ωb/V is the reduced frequency, and C(k) = F + iG is the Theodorsen function. Upon assuming harmonic motion about some centershift α_c as in Eq. (17), the above gives the harmonic coefficients of Eq. (18) as,

$$C_{MI} = \frac{\pi}{2}\left[G + \frac{k}{2}(F-1)\right]A \tag{24}$$

$$C_{MR} = \frac{\pi}{2}\left[F - \frac{k}{2}G + \frac{k^2}{8}\right] \tag{25}$$

$$C_{MO} = \frac{\pi}{2}\alpha_c \tag{26}$$

This linear theory solution is also shown in Figs. 7a, 8a, 9a. The C_{MI} is always negative (always stable) and seems to agree reasonably with the experimental curve for $A=10^{\circ}$. The large increase in C_{MR} at low values of $V/\omega b$ is due to the virtual mass (the $k^2/8$ term in Eq. (25)), and would be absent if virtual mass $I_v\dot{\alpha}$ were neglected. The resulting dimensioned moment M_R remains small as $V \to 0$ due to multiplication of C_{MR} by dynamic pressure $\rho V^2/2$.

A theoretical estimate of the harmonic coefficients C_{MR} and C_{MO} can also be made based on quasi-static aerodynamic consideration using the static moment characteristics shown in Fig. 2. This estimate would assume that under dynamic conditions, the moment coefficient C_M still varies with α as shown in Fig. 2, i.e., there is no dynamic stall overshoot. Assuming harmonic motion about some centershift α_c as in Eq. (17), one can determine the instantaneous C_M as a function of time and then Fourier analyze it to obtain the average component C_{MO} and the fundamental harmonic component C_{MR}. This is described in Ref. 1, and results are shown there for a wide variety of centershifts α_c and amplitudes A. The appropriate quasi-static values of C_{MR} are shown in Figs. 8a-d on the right hand side. These are of course independent of $V/\omega b$ and hence would appear as straight lines. The experimental values of C_{MR} are considerably greater than the quasi-static ones, thereby indicating considerably more aerodynamic moment present than would be expected from simple quasi-

static theory. This is probably due to dynamic stall overshoot effects. For large $V/\omega b$ (i.e., slow oscillations), the quasi-static values appear as possible asymptotes to the experimental results. The appropriate quasi-static C_{MO} curves are shown in Figs. 9a-e. These experimental values of C_{MO} agree reasonably with the quasi-static ones at low amplitudes, but seem to show somewhat more moment at the higher amplitudes, again probably due to dynamic overshoot effects.

The general C_{MI}, C_{MR}, C_{MO} moment coefficient curves given in Figs. 7a-d, 8a-d, 9a-e define the basic nondimensional characteristics of stall aerodynamics for this flat plate wing. From these C_{MI}, C_{MR}, C_{MO} curves, one can then obtain either the transient decay-growth characteristics or the steady limit cycle flutter oscillations for other physical situations -- different sizes, inertias, springs, and dampings. To obtain the transient decay - growth characteristics, one rearranges Eqs. (19), (20), (21) to the form,

$$\frac{\omega_N}{\omega} = \sqrt{\frac{I_T}{I} + \frac{1}{2\mu}\left[\frac{C_{MR}}{A}\left(\frac{V}{\omega b}\right)^2 - \frac{8 I_V}{\rho S c^3}\right]} \tag{27}$$

$$\zeta_T = \frac{I}{I_T}\left[\zeta_F \frac{\omega_N}{\omega} - \frac{C_{MI}}{4\mu A}\left(\frac{V}{\omega b}\right)^2\right] \tag{28}$$

$$\alpha_o = \alpha_c - \frac{C_{MO}}{2\mu\left(\omega_N/\omega\right)^2}\left(\frac{V}{\omega b}\right)^2 \tag{29}$$

$$V = \frac{\omega_N b}{\left(\omega_N/\omega\right)}\left(\frac{V}{\omega b}\right) \tag{30}$$

One first uses Eq. (7) to estimate the virtual Inertia I_V. If I_V/I is small (less than say 5%) one may set $I_V=0$ in the above. For a given amplitude A, centershift α_c, and reduced velocity

$V/\omega b$, one can determine C_{MI}, C_{MR}, C_{MO}. Then from Eqs. (27)-(30) one finds ω_N/ω, ζ_T, α_o, and V. By varying $V/\omega b$, one can obtain a plot of ζ_T versus V for a given amplitude A. To obtain the stall flutter limit cycle, one continues to vary $V/\omega b$ in the above process until one obtains $\zeta_T=0$. This then gives the velocity V for the given limit cycle amplitude A. It can be seen from Eq. (28) that for no friction damping present, $\zeta_F=0$, the flutter point will occur at that $V/\omega b$ where C_{MI} first becomes positive.

The above procedure was actually carried out using the basic C_{MI}, C_{MR}, C_{MO} data to reproduce reasonably the basic wing, the increased inertia, and the increased spring curves given in Figs. 4a, b, c. In doing this, use was made of the basic wing data given in Figs. 5 and 6. Additionally, calculations were made for the three wing cases with no friction damping present, $\zeta_F=0$. The results are shown in Fig. 10. For no friction damping $\zeta_F=0$, increasing the spring rate shifts the velocities proportionally to the natural frequency ω_N. Increasing the inertia also shifts the velocities roughly proportionally to ω_N, but there may be some slight shape change due to the inertia ratio μ which affects the ω_N/ω value. The addition of some friction ζ_F can change the results considerably. The increased inertia case seems to be most affected by the addition of friction ζ_F.

In concluding this section, it should be mentioned that the basic C_{MI}, C_{MR}, C_{MO} curves can be obtained either from free transient response tests as here, or from measured force or pressure measurement on an externally forced oscillating wing as in Refs. 11 and 6. The forced method allows more flexibility in covering the required range of parameters. However, it might be argued philosophically that the coefficients deduced from the free transient response tests, particularly when $\zeta_T=0$ as in a steady flutter oscillation, are more physically direct for predicting flutter, since they are deduced from an actually observed flutter situation.

2.3 Effect of Square Leading Edge

To explore the effect of nose bluntness on the stall flutter and static divergence behavior, the flate plate section was pivoted 180 degrees so that the square section faced the stream and the rounded section became the trailing edge.

Test results for the static moment characteristics are shown in Fig. 11 along with the previous basic wing for comparison. The maximum C_M achieved now was somewhat less than for the basic wing and the linear moment curve slope was 1.07 per radian instead of the previous value of 1.39 per radian. These were probably due to the earlier stalling due to the sharper leading edge and the poorer realization of the Kutta condition due to the rounded trailing edge. The corresponding static divergence characteristics are shown in Fig. 12. The experimental values here are roughly similar to that of the basic wing case Fig. 3a, although the $\alpha_o=0$ points seem slightly lower. The agreement with theory is also somewhat poorer here, indicating that either some of the measured angles were a little off, or perhaps the measured C_M curve of Fig. 11 was a little low.

Figure 13a shows the measured steady-state amplitudes of stall flutter. Comparing these with the previous basic case, Fig. 4a, reveals the same general characteristics for the two cases. The lower amplitudes of the $\alpha_o=5^o$ case do seem to occur at a slightly lower velocity than the basic wing case, but the same two different amplitude limit cycles occur here as before. Figure 13b shows the flutter amplitudes for larger initial angles of attack, $\alpha_o=20^o$ to 90^o, for general interest. Beyond $\alpha_o=50^o$, no limit cycle amplitudes smaller than 90^o could be found, although larger ones were present. For $\alpha_o=90^o$, two different amplitude limit cycle branches occur, one with amplitudes around 100^o and another around 145^o. To obtain these, large disturbances $\Delta\alpha > 90^o$ had to be given to the wing. Incidentally, similar behavior as above occurs for the basic wing, although this was not reported fully in Ref. 1.

In summary then, it appears that the effect of nose bluntness on the stall flutter and static divergence behavior is relatively minor for this flat plate. This is probably to be expected for the relatively low thickness ration, 6.3%, occurring here. For thicker flat plates, the effect may be greater.

SECTION 3

BENDING-TORSION STALL FLUTTER OF A WING SECTION

3.1 Experiment

A preliminary investigation was made into the bending-torsion flutter of a wing section. The experimental set-up is shown in Fig. 14. The same small wind tunnel was used here as for the purely torsional stall flutter investigation of Section 2. The easily removable wood panel, 38.1-cm. x 38.1 cm. square, was replaced by another such wood panel which now had the bending-torsion supporting assembly attached to it. This supporting assembly consisted of a vertical rod which slid up and down between two bearings 10.2 cm. apart to provide the translational motion, and a rotation bearing in the center of the rod to provide the rotational motion. The translation motion was restrained by two linear springs, and the rotational motion was restrained by an .066-cm. diameter steel wire acting in torsion. Both the translational motion and the rotational motion could be locked out independently by an appropriate set screw. The vertical position was measured by a strain gage at the base of a small, very flexible cantilever steel beam whose free end was attached near the upper end of one of the linear springs (where the linear spring motion was small). The angular position was measured by a potentiometer. Also, vertical lines as well as angular lines were drawn on the inside wall of the tunnel for visual observation of the vertical and angular position. The initial angle of attack could easily be varied by changing the clamping position of the .066-cm. diameter restraining torsional wire. A picture of this supporting assembly is shown in Fig. 14b.

The two-dimensional wing section was a roughly symmetrical 0012 airfoil section with a 12.70-cm. chord and a 1.52-cm. thickness, which was pivoted about the quarterchord. A small weight was placed in the wing section at about the midchord to give a

substantial static unbalance. The wing had a small rod at its quarterchord by which it could be attached to the supporting assembly. In doing this attaching, a slot had to be provided in the tunnel wall to allow the wing to translate vertically. To minimize the leakage around the slot, a rubber membrane with a thin slit was placed over the slot to close the gap around the moving rod. Also, a thin aluminum disk about 13.0-cm. in diameter was placed at the base of the airfoil to help prevent pressure leaking from one side of the airfoil to the other through the tunnel slot. Measured values of the wing section and its static and dynamic properties are given in Fig. 15.

Static tests were first carried out to measure the aerodynamic lift and moment acting on the wing section. The .066-cm. diameter torsional spring wire was replaced by a much thicker .318-cm. diameter wire and an appropriate strain gage to measure torsional moment, while the vertical position strain gage on the restraining linear spring was used to measure the spring deflection and hence lift force on the wing. The angle of attack was varied in small steps and readings were always taken with wind on and wind off to measure the resulting increments in force and moment due to the aerodynamics. As mentioned in Section 2, because of blockage in the tunnel, the velocity for this and any of the subsequent test runs was always defined as the velocity registered by the tunnel manometer when the wing section was brought to zero manually and the variac power setting for the wind tunnel motor was not changed.

Figures 16 and 17 show the measured static lift and moment characteristics of the airfoil section. The lift curve shows a linear lift curve slope of 5.35 per radian, which agrees reasonably with the theoretical value of 6.28 per radian, and stalling occurring at about +14 degrees and -13 degrees. The moment curve shows an essentially zero moment in the same unstalled region and a large negative restoring moment outside it. There is a substantial discontinuity occurring at the stalling points.

The zero moment in the linear range again agrees with theory for a symmetrical wing section pivoted about the quarter chord. It should be mentioned that before the pressure leakage around the slot was minimized by the thin aluminum disk referred to earlier, the lift curve measurements indicated somewhat of a discontinuity in angle around α=0 degrees and a much lower average lift curve slope of about 2.5 per radian.

The spring rates for the translation and rotation restraining springs were measured next. The translation spring was found to be linear over its entire range with a spring rate of 139 N/m, while the torsional spring had the nonlinear characteristics shown in Fig. 18. These nonlinear characteristics are due to gravity effects of the static unbalance of the wing section and will be discussed in the next section. When the wing was oriented vertically instead of horizontally so that no gravity moment acted, the measured torsional spring was linear over its entire range with a spring rate of .0137 N-m/rad.

The static equilibium characteristics of the wing section are shown in Fig. 19. These were obtained by first locking out the translational motion of wing, then giving the wing a specified initial angle of attack α_o, and then observing visually the resulting static angles α_s as the tunnel velocity was increased in small increments. The measurements generally show a decrease in angle of attack as the velocity is increased, which reflects the stable moment curve characteristics given by Fig. 17. It should be mentioned that when the static angles α_s came in the neighborhood of about 14 degrees (the stall region), small amplitude torsional oscillations developed. These will be discussed again later.

The bending-torsion stall flutter characteristics of the wing section were investigated by giving the wing a specified angle of attack α_o, and then varying the tunnel velocity in small increments from 0 to 15 m/sec. Before each run, static calibrations of the translational and angular positions were

taken, and also dynamic transient decay responses were taken of the translational motion with the angular motion locked out, and of the angular motion with translation locked out. From these dynamic tests at zero wind velocity, the natural frequencies in bending ω_h and torsion ω_α were obtained, as well as the critical damping ratios ζ_h and ζ_a for the wing section. These dampings here represent bearing friction plus air damping and were relatively high here, about $\zeta_h \simeq .15$ and $\zeta_\alpha \simeq .13$ respectively. Because of the preliminary nature of this investigation, a careful attempt at extracting the purely bearing friction was not made here, as was done for the purely torsional flutter of Section 2. In subsequent investigations such attempts would be made along with a general reduction of the high friction levels found in these tests.

At each given wind velocity during a test run, the wing section was given a small disturbance Δh in the translation position and then let go to see if flutter would ensue. In general, the flutter was not self-excited because of the large friction present, except at the higher velocities. Figure 20 shows a typical photograph of the wing section during flutter. The large bending and torsion amplitudes obtained here are well into the stalling range of the airfoil. Figures 21a and 21b show the measured bending and torsion amplitudes for initial angles of attack $\alpha_o=0^o$ and 20^o respectively. Aside from the large oscillation amplitudes here, it is interesting to notice that the torsion amplitude decreases with velocity after having achieved a peak value. This changes the general appearance of the flutter oscillation with velocity. Also, it appears here that the flutter started in at a slightly higher velocity at $\alpha_o=20^o$ than it did at $\alpha_o=0^o$.

In addition to this large amplitude bending-torsion stall flutter, a small amplitude predominantly torsional flutter was observed when the wing section was rotated such that the resulting static equilibrium angle α_s was about 14 degrees. This "small stall" flutter had an amplitude of about 3.5 degrees and existed even if the bending degree of freedom was locked out. It was

evidently related to the stalling of the wing section and the associated sharp change in C_M. See Fig. 17. When bending motion was permitted as well, the torsional amplitude became more regular and somewhat larger. The flutter amplitudes for this "small stall" flutter are shown in Fig. 21c, with and without the bending degree of freedom.

The flutter frequencies for the large amplitude bending-torsion flutter and the "small stall" flutter are shown in Fig. 22. The large amplitude flutter frequencies vary from 4.0 to 4.7 H_z which is somewhat above the natural frequencies of ω_h = 3.81 and ω_α = 2.55 Hz. The "small stall" flutter frequencies varied from 4.5 to 7.8 Hz which was considerably above the torsional natural frequency ω_α = 2.55 Hz. This was due to the stiffening effect of the aerodynamic moment at the stall region, as will be shown later.

For interest, the "small stall" flutter was investiaged further by varying the restraining torsional spring of the wing section. Figure 23 shows the resulting flutter frequencies. As expected, increasing ω_α increased the resulting flutter frequencies.

3.2 Theory and Discussion

The static aerodynamic characteristics of the airfoil wing section about its quarterchord are expressed by the nondimensional lift and moment coefficients as

$$C_L = \frac{L}{\frac{1}{2}\rho V^2 S} \tag{31}$$

$$C_M = \frac{M}{\frac{1}{2}\rho V^2 S c} \tag{32}$$

For a two-dimensional symmetrical wing section pivoted about the quarterchord, the theoretical lift and moment curve slopes in the linear (unstalled) region are $dC_L/d\alpha$ = 6.28 per radian and $dC_M/d\alpha$ = 0 respectively. These agree reasonably with the measured values given in Figs. 16 and 17.

The static equilibrium positions in torsion can be evaluated from the nonlinear moment equilibrium equation,

$$\tfrac{1}{2}\rho V^2 S c\, C_M(\alpha) = M_s(\alpha) - M_s(\alpha_o) \qquad (33)$$

where C_M is the nonlinear aerodynamic moment coefficient shown in Fig. 17 and M_s is the nonlinear spring moment shown in Fig. 18. Equation (33) can be solved by trial and error for the resulting equilibrium angle α_s. For the present investigation, the experimental results for α_s given in Fig. 19 were used to reconstruct the nonlinear C_M versus α curve given in Fig. 17, by simply solving Eq. (33) for C_M. Good agreement with the measured C_M curve was obtained, thereby providing a cross-check on the measured C_M values.

The stall flutter characteristics of the wing section oscillating through large angles, can be represented by the equations of motion,

$$m\ddot{h} - S_\alpha \ddot{\alpha} \cos\alpha + S_\alpha \dot{\alpha}^2 \sin\alpha + k_h h = L_{aero} - gm \qquad (34)$$

$$-S_\alpha \ddot{h} \cos\alpha + I\ddot{\alpha} + k_T(\alpha - \alpha_i) = M_{aero} + g S_\alpha \cos\alpha \qquad (35)$$

where m and I represent the total mass and moment of inertia, respectively, of the wing section plus associated moving support assembly parts, S_α is the mass static unbalance of the wing, k_h is the bending spring rate, k_T is the torsion spring rate, and α_i is the angular position for no torsion spring moment. The above equations were obtained by applying Lagrange's equations to the wing section. The gravity term in Eq. (34) simply represents a constant displacement shift and can be discarded. However, the gravity term in Eq. (35) should be included in the left hand side, and hence, Eq. (35) can be rewritten as,

$$-S_\alpha \ddot{h} \cos\alpha + I\ddot{\alpha} + M_s = M_{aero} \qquad (36)$$

where M_s represents a nonlinear spring restoring force defined as,

$$M_s = k_T \left(\alpha - \frac{g S_\alpha}{k_T} \cos\alpha - \alpha_i \right) \tag{37}$$

For values of gS_α/k_T close to 1, a significant nonlinearity develops in the spring rate. In fact, for $gS_\alpha/k_T > .1$ there will be a buckling snap-through for the torsional spring. For the present case, $gS_\alpha/k_T = .710$ and only a mild nonlinearity develops. The measured nonlinear spring moment M_s versus α is shown in Fig. 18 and it agreed well with the theoretical prediction of Eq. (37).

If one assumes harmonic motion for the wing section of the form,

$$\begin{aligned} h(t) &= h_c + A_h e^{i\omega t} \\ \alpha(t) &= \alpha_c + A_\alpha e^{i\omega t} \end{aligned} \tag{38}$$

then the aerodynamic lift and moment appearing in Eqs. (34) and (36) can be expressed in harmonic form as,

$$\begin{aligned} L_{aero} &= \tfrac{1}{2}\rho V^2 S \left[C_{LO} + (C_{LR} + i C_{LI}) e^{i\omega t} \right] \\ M_{aero} &= \tfrac{1}{2}\rho V^2 S c \left[C_{MO} + (C_{MR} + i C_{MI}) e^{i\omega t} \right] \end{aligned} \tag{39}$$

where the six harmonic coefficients C_{LO}, C_{LR}, etc. are assumed to be functions of amplitudes A_h, A_α, centershift α_c, and reduced frequency $\omega b/V$. As an approximation, the six coefficients can be further divided into twelve by assuming independence of the h and α effects, namely,

$$\begin{aligned} C_{LR} &= C_{LhR} + C_{L\alpha R} \\ C_{LI} &= C_{LhI} + C_{L\alpha I} \end{aligned} \tag{40}$$

etc.

where the C_{LhR}, C_{LhI}, ... are assumed to depend only on A_h, α_c, and $\omega b/V$ while the $C_{L\alpha R}$, $C_{L\alpha I}$, ... are assumed to depend only on A_α, α_c and $\omega b/V$.

Placing Eqs. (38) and (39) into the flutter Eqs. (34) and (36) and using a harmonic balance scheme, one can obtain a set of six nonlinear equations which can be solved by some Newton-Raphson type iteration scheme to obtain the amplitudes and frequencies of the nonlinear stall flutter. This, however, was not pursued further in this preliminary investigation.

A standard, linear flutter analysis of this typical section was performed to obtain an idea of its basic, small amplitude flutter characteristics. Following Ref. 19, and using the measured properties indicated in Fig. 15, the following standard nondimensional flutter parameters were computed as,*

$$\tilde{\mu} = \frac{m}{\pi \rho b^2 \ell} = 290 \qquad a = -.5$$

$$x_\alpha = \frac{S_\alpha}{m b^2} = .065 \qquad \frac{\omega_h}{\omega_\alpha} = 1.50 \tag{41}$$

$$r_\alpha = \sqrt{\frac{I}{m b^2}} = .259$$

These were then placed into the flutter determinant (for a = -.5),

$$\begin{vmatrix} \tilde{\mu}\left[1 - \left(\frac{\omega_h}{\omega_\alpha}\right)^2 Z_3\right] + L_h & \tilde{\mu} x_\alpha + L_\alpha \\ \tilde{\mu} x_\alpha + \frac{1}{2} & \mu r_\alpha^2 \left[1 - Z_3\right] + M_\alpha \end{vmatrix} = 0 \tag{42}$$

*The high value of $\tilde{\mu}$ reflects the associated assembly support equipment moving with the wing.

where L_h, L_α, M_α are standard aerodynamic coefficients which are functions of reduced frequency $k = \omega b/V$, and the $Z = (1+ig)(\omega_\alpha/\omega)^2$ is the unknown complex eigenvalue. A standard V-g method of solution was used to solve for the flutter speed and frequency. These calculations resulted in the V-g diagram shown in Fig. 24, which gives a zero damping g=0 flutter speed of $V_F = 5.2$ m/sec and a flutter frequency $\omega_F = 3.9$ Hz. However, because of the slowly rising V-g curve for this configuration, the effect of structural damping can be pronounced. For the actual wing here, the measured critical damping ratio at zero velocity was found to be about $\zeta_h \simeq \zeta_\alpha \simeq .15$ as given in Fig. 15. This includes both the bearing function and the aerodynamic damping at zero velocity which was not separated as in the previous torsional investigation of Section 2. Assuming that bearing friction contributes a large part of this damping, one can arbitrarily estimate the friction damping as $\zeta_F \simeq .10$. Then, using the rough relationship,

$$g \approx 2\zeta_F \tag{43}$$

one obtains a rough estimate of about $g \simeq .20$ for the structural damping here. From Fig. 24, this would indicate a flutter speed of $V_F = 10.6$ m/sec and a flutter frequency of $\omega_F = 3.4$ Hz, which agree reasonably with the observed flutter results. Presumably, if the friction level were lower, the flutter would have occurred at a lower velocity, and would have been self-excited.

In contrast to the large amplitude coupled bending-torsion flutter, the "small stall" flutter mentioned earlier seems to involve only the torsion motion of the wing. This seems to be associated with the sharp change in moment at the stalling point and the associated hysterysis in the development and drop-off of the moment. See Fig. 17. See also Ref. 15 for some further details of this phenomenon. The increase in torsional frequency far above the zero velocity natural frequency ω_α can be related

to the stiffening effect of the jump in moment, by considering small oscillations of the wing about the stall position,

$$\alpha - \alpha_{stall} \approx A \sin \omega t \tag{44}$$

The total moment here can be idealized roughly as,

$$M \approx \frac{\Delta M}{2} + k_\alpha (\alpha - \alpha_{stall}) \quad \text{for } \alpha > \alpha_{stall} \tag{45}$$

$$\approx -\frac{\Delta M}{2} + k_\alpha (\alpha - \alpha_{stall}) \quad \text{for } \alpha < \alpha_{stall}$$

where ΔM represents the jump in aerodynamic moment at stall. The above moment M, during an oscillation, can be replaced by its fundamental harmonic component as,

$$M \approx C_1 \sin \omega t \tag{46}$$

where the Fourier coefficient C_1 can be obtained by multiplying Eq. (46) by sin ωt, integrating over a half cycle, and then substituting Eqs. (45) and (44) to give,

$$C_1 = \frac{2\omega}{\pi} \int_0^{\pi/\omega} M \sin \omega t \, dt = \frac{2}{\pi} \Delta M + k_\alpha A \tag{47}$$

The torsional vibrations of the wing are governed by the equation of motion,

$$I \ddot{\alpha} + M = 0 \tag{48}$$

Substituting Eqs. (44) and (46) into the above, solving for the frequency ω and noting that $\omega_\alpha^2 = k_\alpha / I$ gives finally,

$$\omega \approx \sqrt{\omega_\alpha^2 + \frac{\rho V^2 S c}{\pi I A} \Delta C_M} \tag{49}$$

Using the basic parameters of Fig. 15 and taking $\Delta C_M \simeq .09$ and $A \simeq 3.5$ degrees, the above Eq. (49) gives a reasonable estimate of the "small stall" flutter frequency, as shown in Fig. 22.

SECTION 4

CONCLUSIONS

The investigation of the torsional stall flutter and nonlinear divergence behavior of a flat plate pivoted about its midchord, revealed the following observations.

1. The nonlinear static divergence equilibrium properties were accurately predicted from the measured static moment characteristics of the plate. Good nondimensional correlation was obtained for several wing configurations. Above the linear divergence speed, the static divergence characteristics resembled the buckling of a flat plate with initial imperfections.
2. Large amplitude limit cycles ranging from $\pm$ 11 to $\pm$ 160 degrees were observed. In some cases, two different limit cycles were found for the same velocity.
3. Stall flutter occurred above a critical value of around $V/b\omega \tilde{\sim} 2$. It seemed to be initiated if the wing angle of attack came near the stall angle, either by a sufficiently large disturbance (for high initial angles α_o) or by the natural divergence process (for low α_o).
4. Nondimensional harmonic coefficients C_{MI}, C_{MR}, C_{MO} were extracted from the free transient vibration tests for amplitudes up to 80 degrees. Reasonable nondimensional correlation was obtained for several wing configurations. From these basic curves, one could obtain the steady-state and transient behavior of other spring, inertia, and damping configurations.
5. The effect of nose bluntness on the static divergence and stall flutter behavior was found to be relatively minor for the 6.3% thickness ratio flate plate investigated here.

The preliminary investigation of the bending-torsion stall flutter and nonlinear static divergence behavior of an airfoil

wing section pivoted about its quarterchord, revealed the following observations.

1. The nonlinear static equilibrium angles could be well predicted from the measured static moment characteristics of the wing.
2. Care had to be taken to prevent pressure leakage from one side of the wing to the other through the wing holding mechanism.
3. Large amplitude coupled limit cycles were observed, with torsion amplitudes as large as $\pm$ 40 degrees. The torsion amplitudes first increased, then decreased with increasing velocity. The occurrence of coupled mode flutter was reasonably predicted by linear theory.
4. Because of large friction present, the stall flutter was not self-excited, except at the higher velocities. Generally, a sufficiently large disturbance was necessary to initiate it.
5. In addition to the large amplitude bending-torsion flutter, a small amplitude, predominantly torsional flutter was observed when the static equilibrium angle of the wing was at the stall point. The amplitude here was about $\pm$ 3.5 degrees, and the frequency was much higher than the natural frequency at zero speed due to the stiffening effect of the aerodynamic moment at the stall.

The above preliminary investigation of bending-torsion could be extended further to explore the phenomenon in more depth. In future work, more care should be taken to lower the high friction levels present, and to lower the associated assembly support moving mass in order to make the density ratios $\tilde{\mu}$ more typical of actual construction. Also, the bending to torsion frequency ratio should probably be lower.

Because of tunnel blockage, the absolute velocities and coefficients for the torsional flutter and the bending-torsion flutter tests here may not be accurate, but the general trends and

phenomena should be similar on other wing sections. It is hoped the present report has contributed some further information and understanding to the interesting and complicated phenomenon of nonlinear stall flutter.

REFERENCES

1. Dugundji, J., and Aravamudan, K., Stall Flutter and Nonlinear Divergence of a Two-Dimensional Flate Plate Wing, M.I.T. Aeroelastic and Structures Research Laboratory Report ASRL TR 159-6, Air Force Office of Scientific Research, AFOSR TR 74-1734, July 1974.

2. Victory, M., "Flutter at High Incidence", BRitish A.R.C. R.&M. 2048, January 1943.

3. Bratt, J.B., and Wight, K.C., "The Effect of Mean Incidence, Amplitude of Oscillation, Profile and Aspect Ratio on Pitching Moment Derivatives", British A.R.C. R.&M. 2064, June 1945.

4. Halfman, R.L., Johnson, H.C., and Haley, S.M., "Evaluation of High-Angle-of-Attack Aerodynamic-Derivative Data and Stall-Flutter Prediction Techniques", NACA TN 2533, November 1951.

5. Rainey, A.G., "Preliminary Study of Some Factors Which Affect the Stall-Flutter Characteristics of Thin Wings", NACA TN 3622, March 1956.

6. Rainey, A.G., "Measurement of Aerodynamic Forces for Various Mean Angles of Attack on an Airfoil Oscillating in Pitch and on Two Finite-Span Wings Oscillating in Bending with Emphasis on Damping in the Stall", NACA Report TR 1305, 1957.

7. Parkinson, G.V., and Smith, J.D., "Square Prism as an Aeroelastic Non-linear Oscillator", Quarterly J. of Mechanics and Appl. Math., Vol. 17, Part 2, November 1964, pp. 225-239.

8. Vickery, B.J., "Fluctuating Lift and Drag on a Long Cylinder of Square Cross Section in a Smooth and in a Turbulent Stream", J. of Fluid Mechanics, Vol. 25, Part 3, 1966, pp. 481-494.

9. Novak, M., "Galloping Oscillation of Prismatic Structures", J. of Eng. Mechanics Division, EM-1, Proc. of ASCE, February 1972.

10. Otsuki, Y. and Washizu, K., "Flutter Experiments on Prismatic Bars of Rectangular Sections", Proceedings of Sixteenth Japan National Congress for Applied Mechanics 1966, pp. 211-214.

11. Otsuki, Y., Washizu, K., Tomizawa, H., and Ohya, A., "A Note on the Aeroelastic Instability of a Prismatic Bar with Square Section", Journal of Sound and Vibration, Vol. 34, No. 2, 22 May 1974, pp. 233-248.

12. Ham, N., "Aerodynamic Loading on a Two-Dimensional Airfoil During Dynamic Stall", AIAA J., Vol. 6, No. 8, October 1968, pp. 1927-1934.

13. Ericsson, L.E., and Reding, J.P., "Stall-Flutter Analysis", J. of Aircraft, Vol. 10, No. 1, January 1973, pp. 5-13.

14. Carta, F.O., "Analysis of Oscillatory Pressure Data Including Dynamic Stall Effects", NASA CR-2394, prepared by United Aircraft Research Laboratories, May 1974.

15. Crimi, P. and Reeves, B.L., "A Method for Analyzing Dynamic Stall of Helicopter Rotor Blades", NASA CR-2009, prepared by Avco Systems Division, May 1972.

16. Carta, F.O., "Turbomachinery Flutter", United Aircraft Research Laboratories Report UAR-J242, October 20, 1970.

17. Crimi, P., "Analysis of Helicopter Rotor Blade Stall Flutter", J. of Aircraft, Vol. 11, No. 7, July 1974, pp. 407-413.

18. Reed, W.H., III, "Wind Effects on Space Shuttle Vehicle Erected on a Launch Pad", Proceedings of the Third International Conference on Wind Effects on Buildings and Structures, Sept. 6-9, 1971, Tokyo, Japan, Saikon Co., Tokyo, 1971, pp. 1127-1140.

19. Bisplinghoff, R.L., Ashley, H., and Halfman, R.L., Aeroelasticity, Addison-Wesley Publishing Co., Reading, Mass., 1955.

20. Den Hartog, J.P., Mechanical Vibrations, McGraw-Hill Book Co., New York, 4th Edition, 1956.

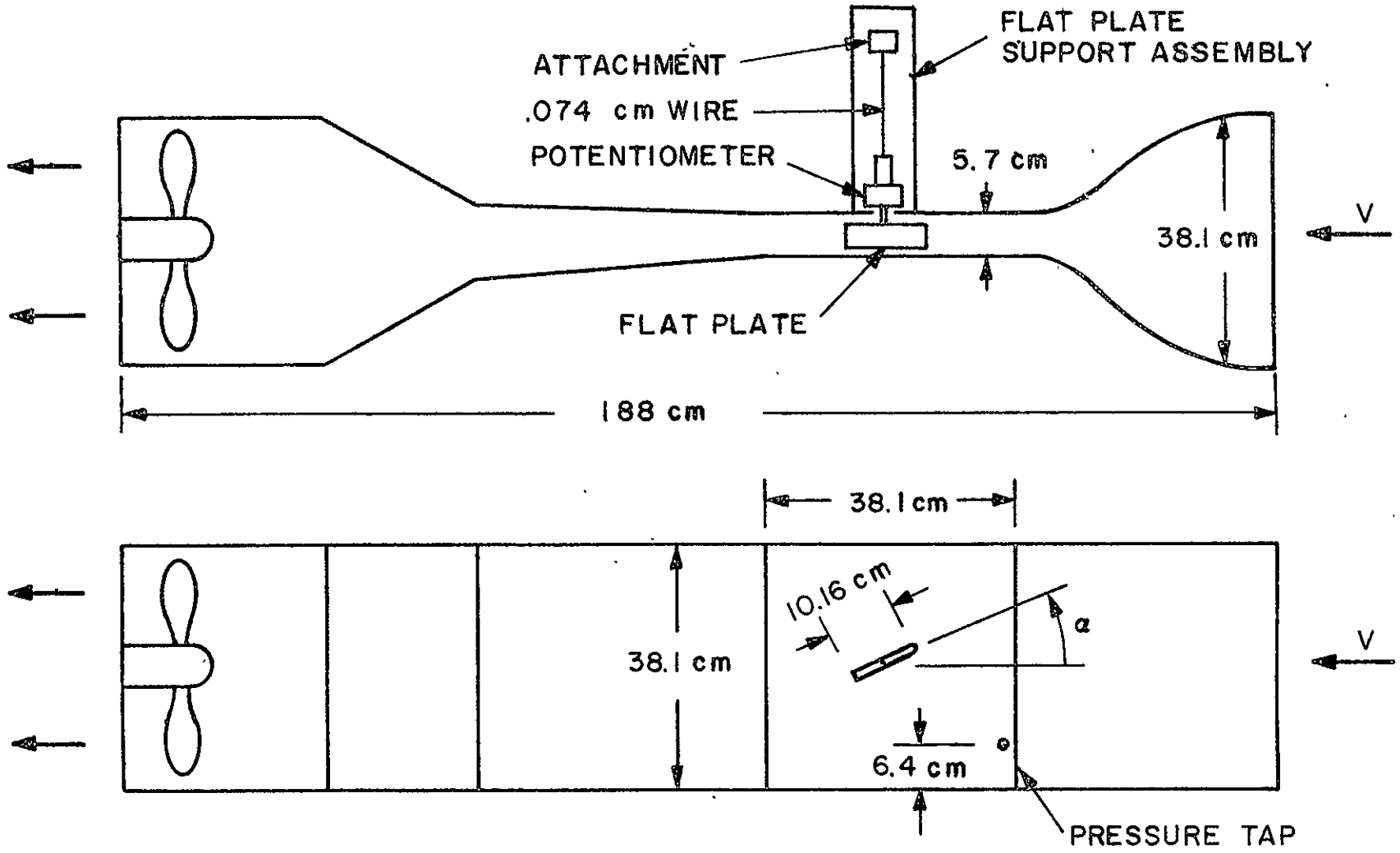

FIG. 1 EXPERIMENTAL SET-UP FOR TORSIONAL STALL FLUTTER

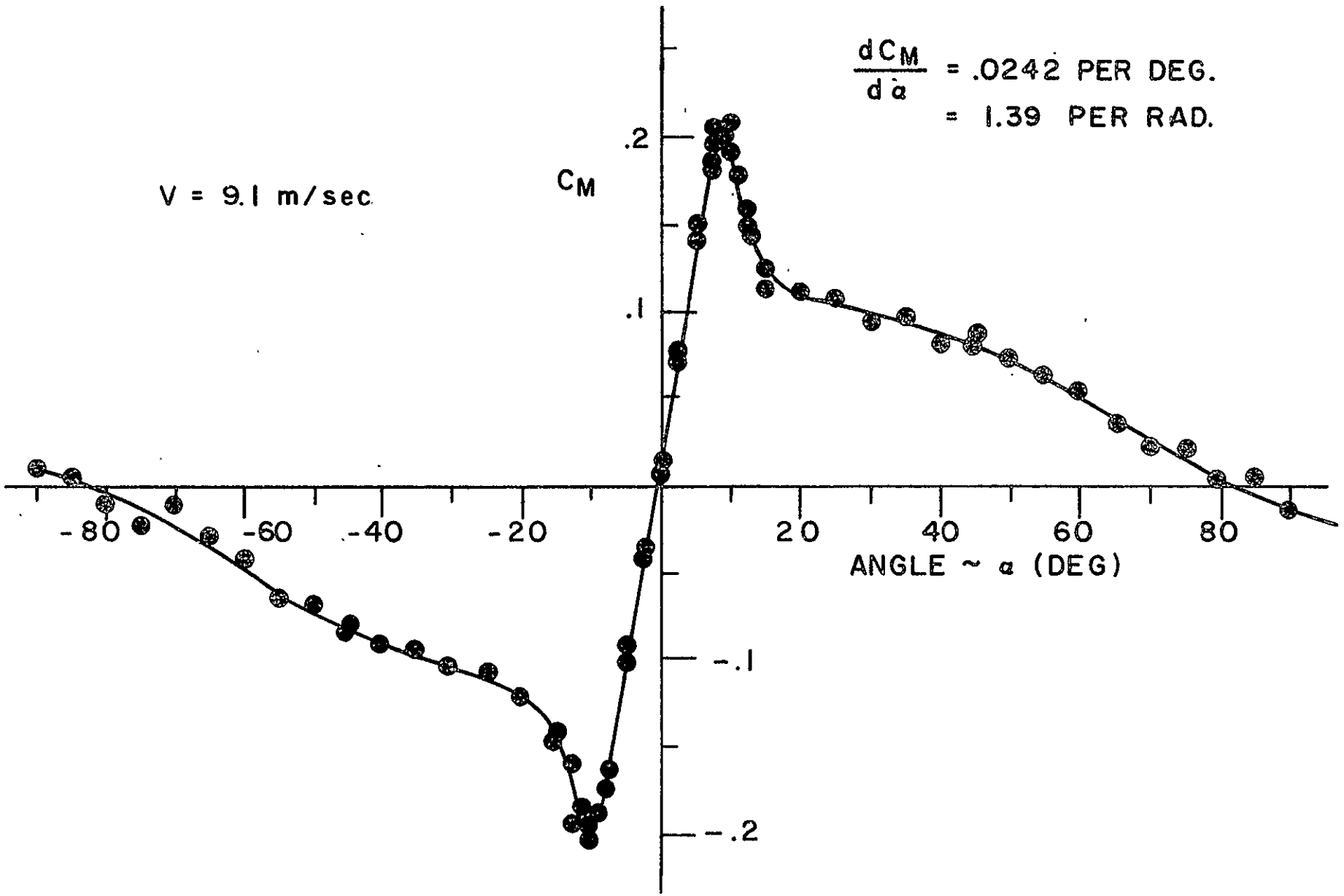

FIG. 2 STATIC MOMENT FOR FLAT PLATE WING

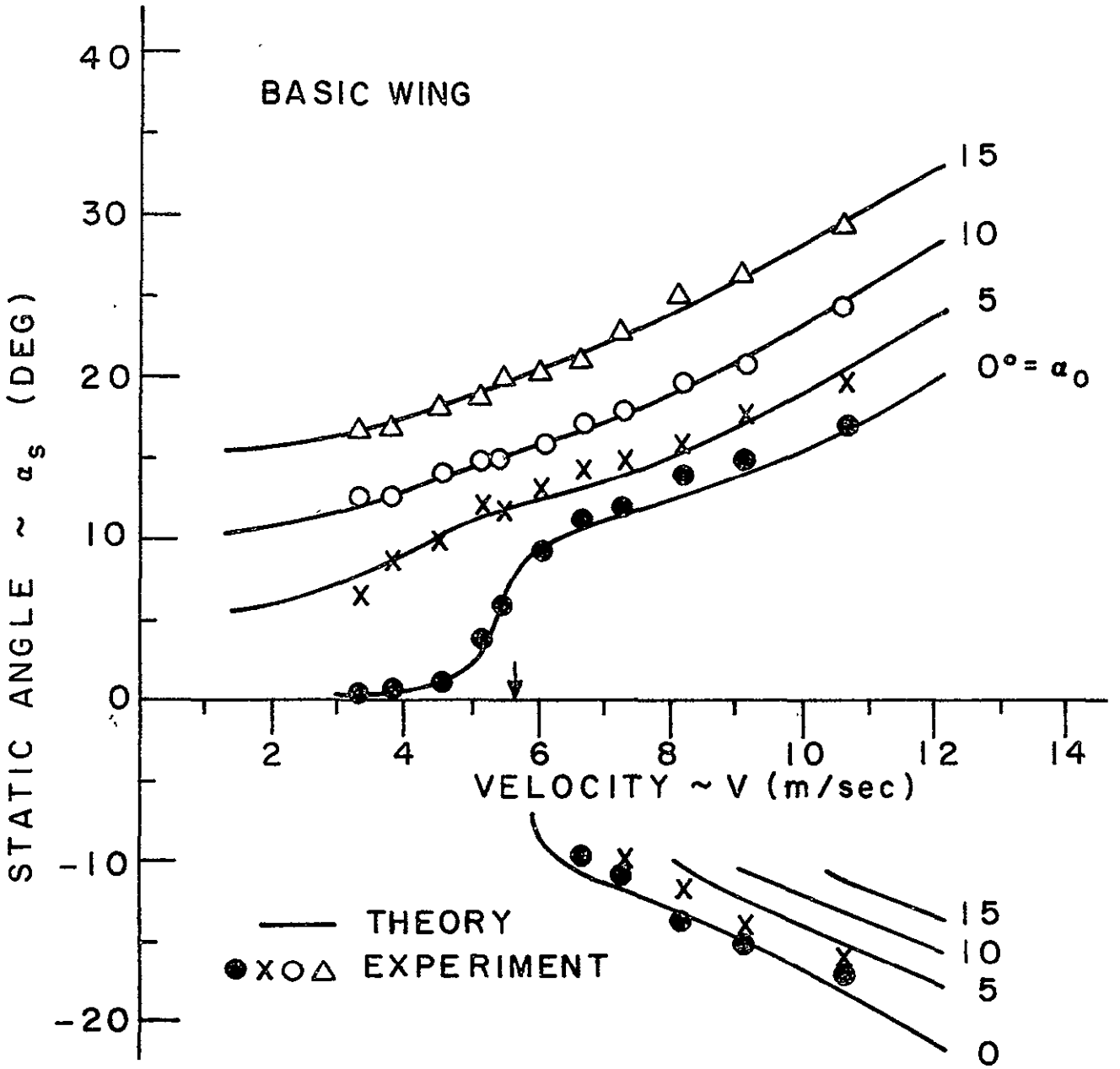

FIG. 3A STATIC DIVERGENCE (BASIC WING)

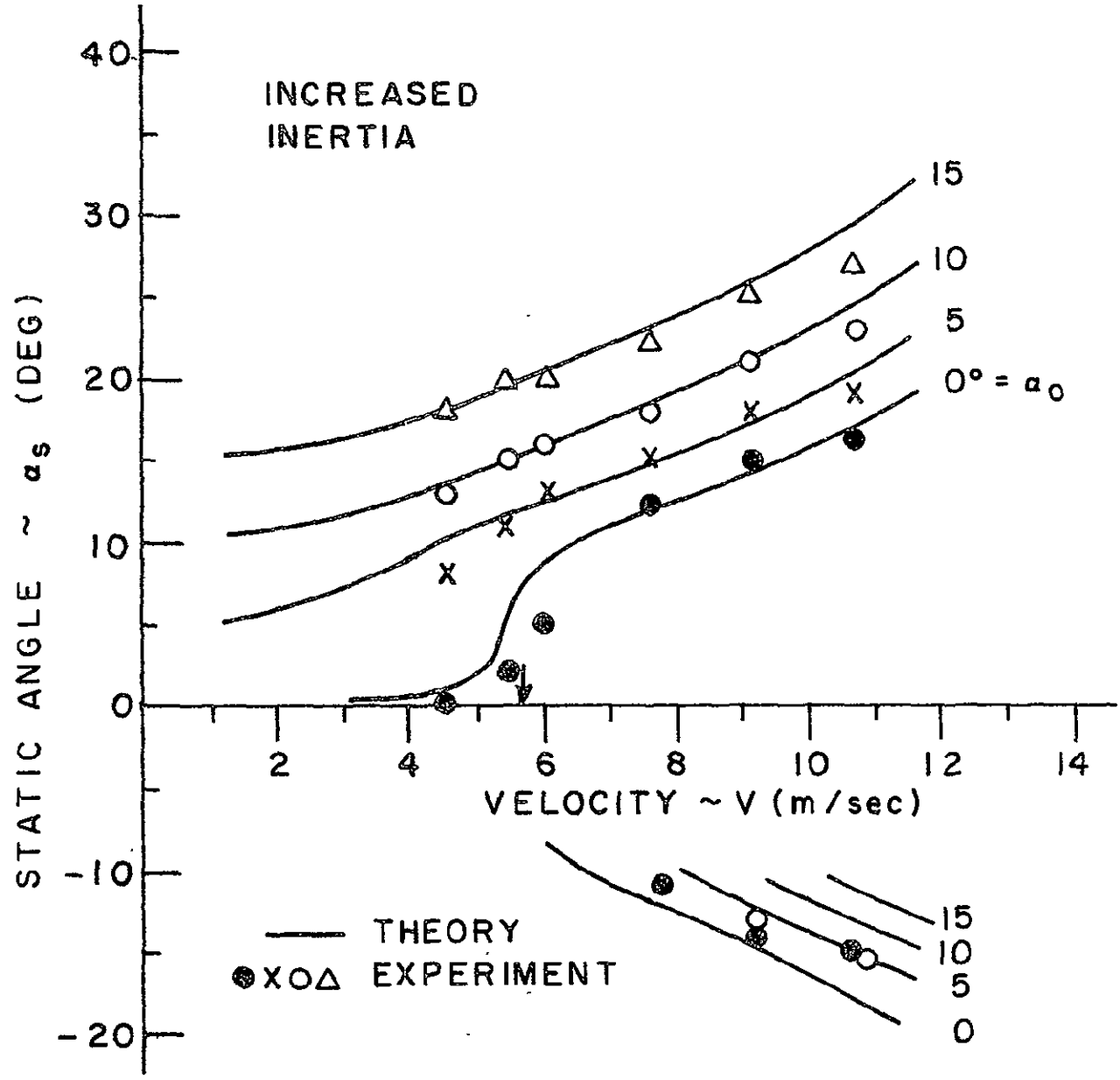

FIG: 3B STATIC DIVERGENCE (INCREASED INERTIA)

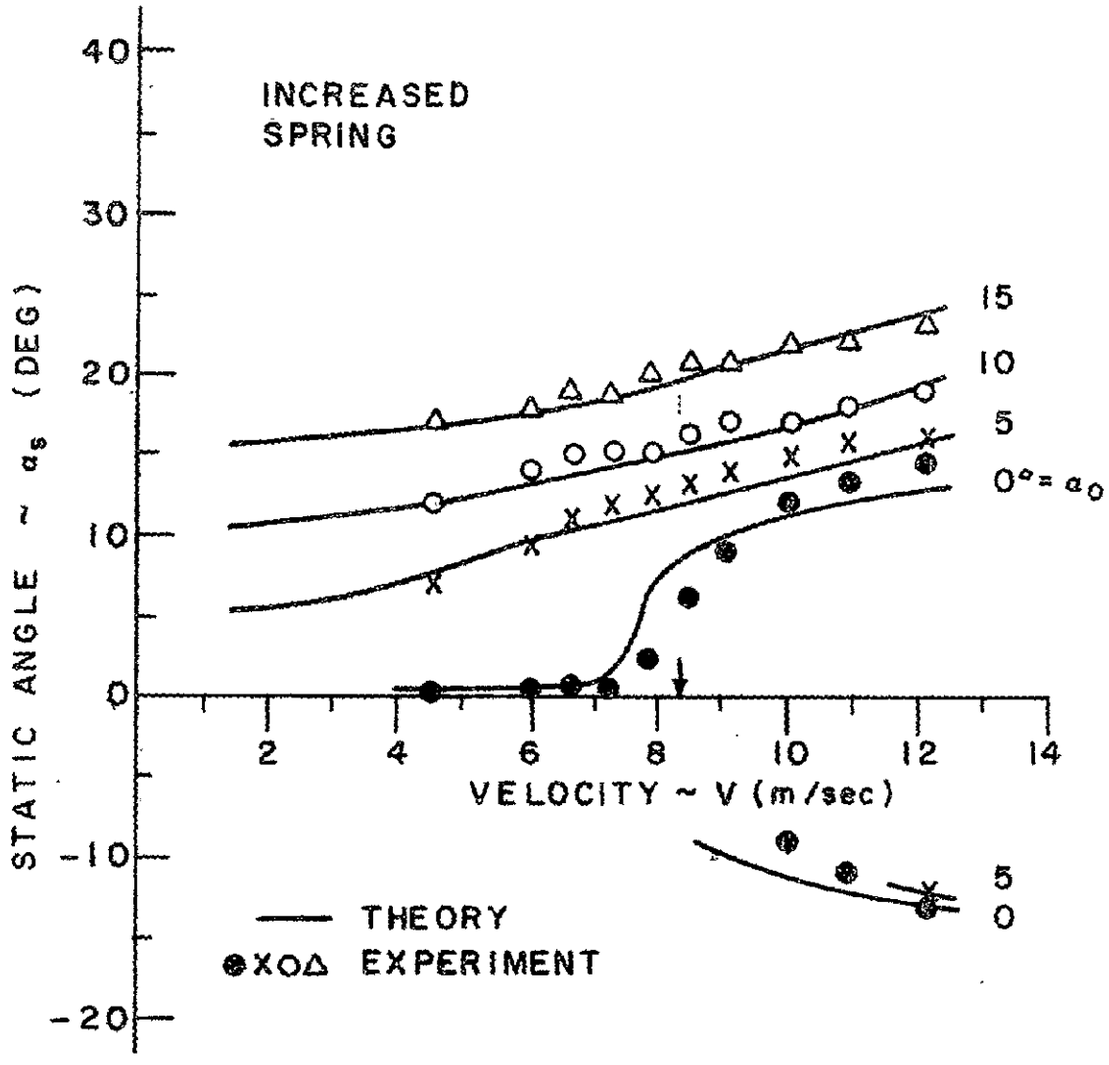

FIG. 3c STATIC DIVERGENCE (INCREASED SPRING)

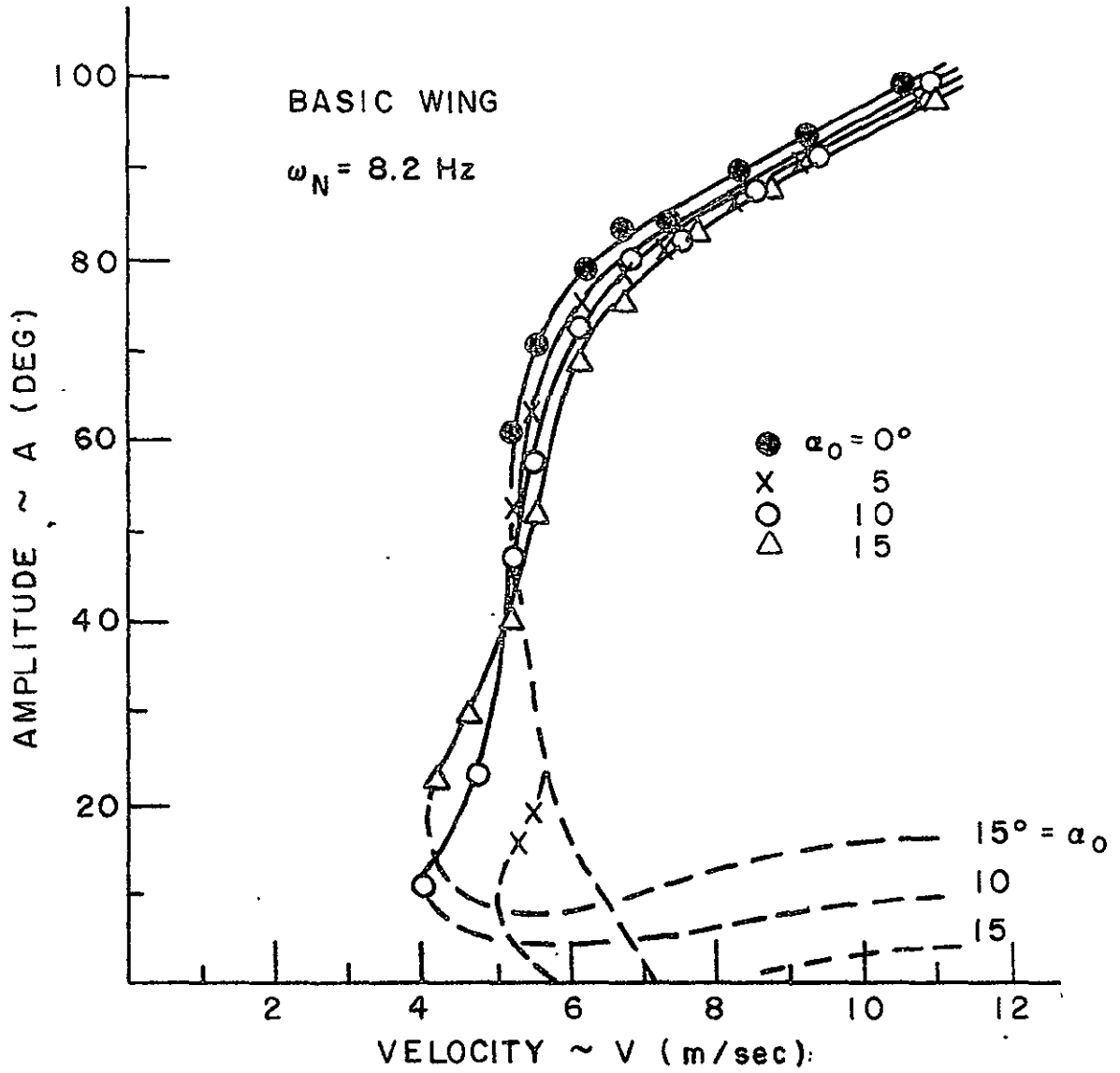

FIG. 4A FLUTTER AMPLITUDES (BASIC WING)

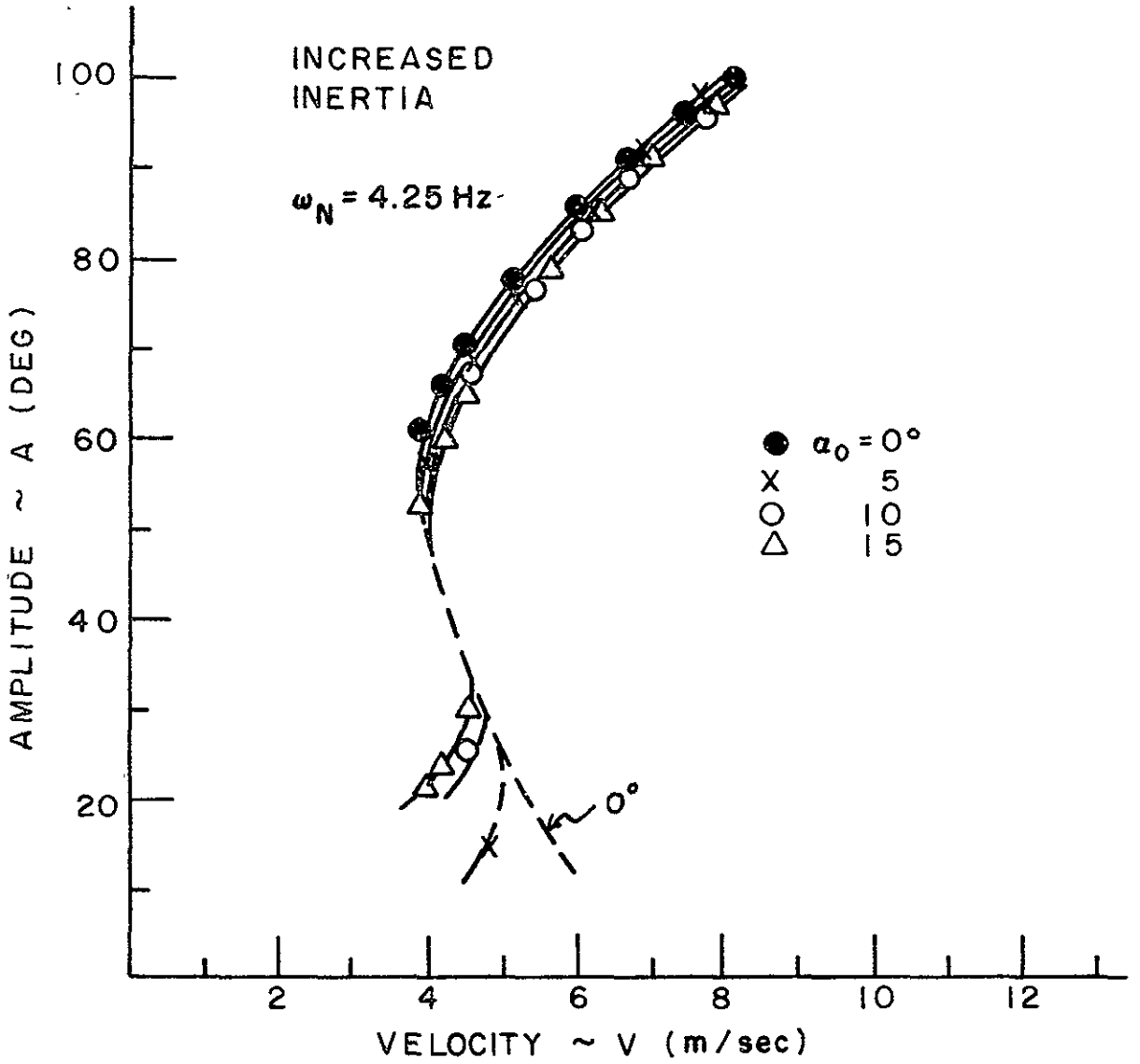

FIG. 4B FLUTTER AMPLITUDES (INCREASED INERTIA)

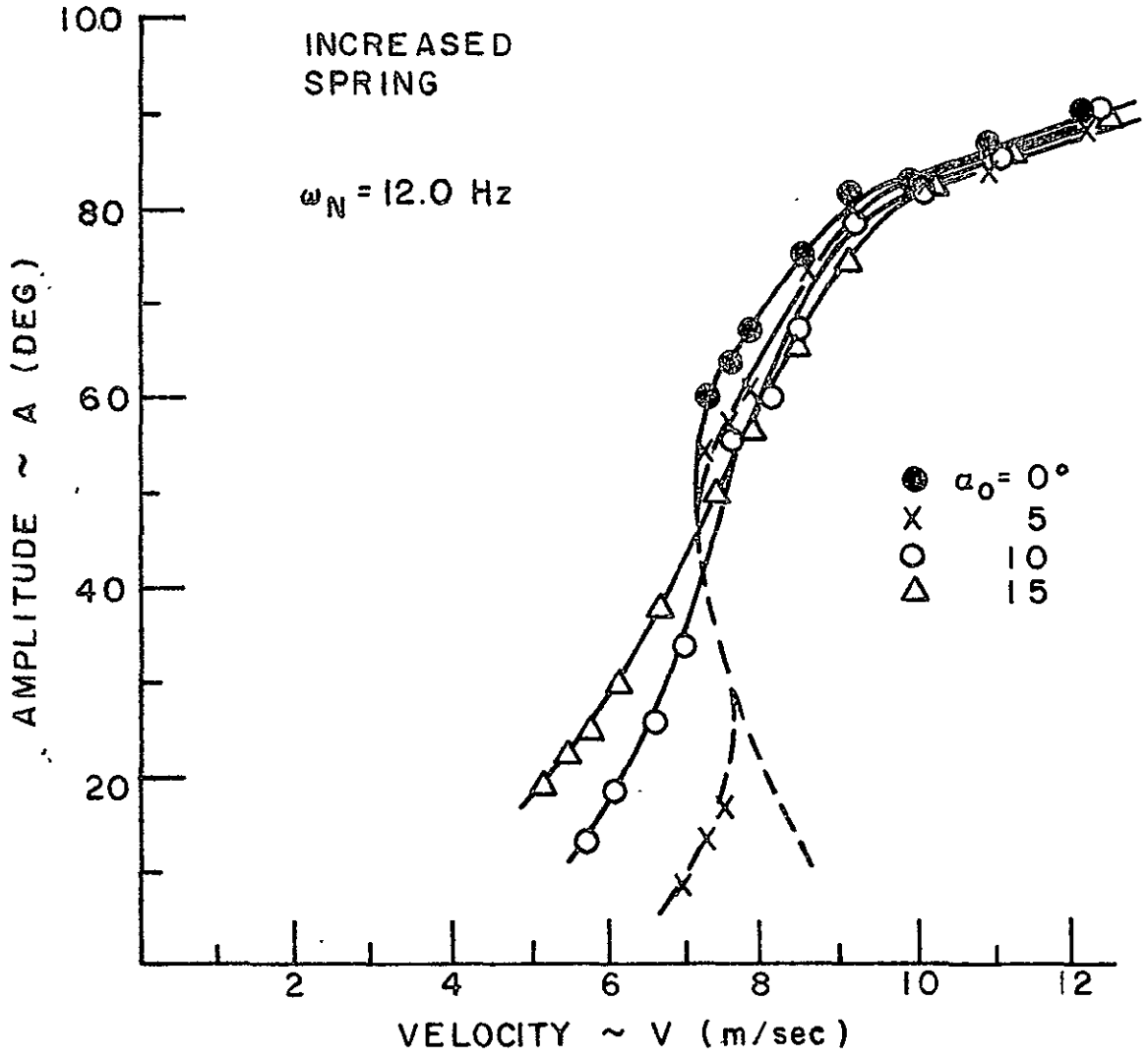

FIG. 4c FLUTTER AMPLITUDES (INCREASED SPRING)

Amplitude A	Basic Wing ζ_F	Increased Inertia ζ_F	Increased Stiffness ζ_F
10°	.035	.041	.019
20	.023	.023	.015
40	.016	.015	.010
60	.012	.013	.009
80	.011	.012	.008

FIG. 5 MEASURED VALUES OF FRICTION DAMPING RATIO

ρ	=	1.226	kg/m^3
S	=	.00549	m^2
c	=	.1016	m
b	=	.0508	m
$\frac{dC_M}{d\alpha}$	=	1.39	per rad.

Wing pivoted about 1/2 chord

Parameter	Basic Wing	Increased Inertia	Increased Spring
k_T (N-m/rad)	.0156	.0156	.0334
I ($kg-m^2$)	5.89×10^{-6}	21.9×10^{-6}	5.89×10^{-6}
μ	3.34	12.43	3.34
ω_N (Hz)	8.2	4.25	12.0
$b\omega_N$ (m/sec)	2.62	1.356	3.83

FIG. 6 PARAMETERS FOR FLAT PLATE WING (TORSIONAL FLUTTER)

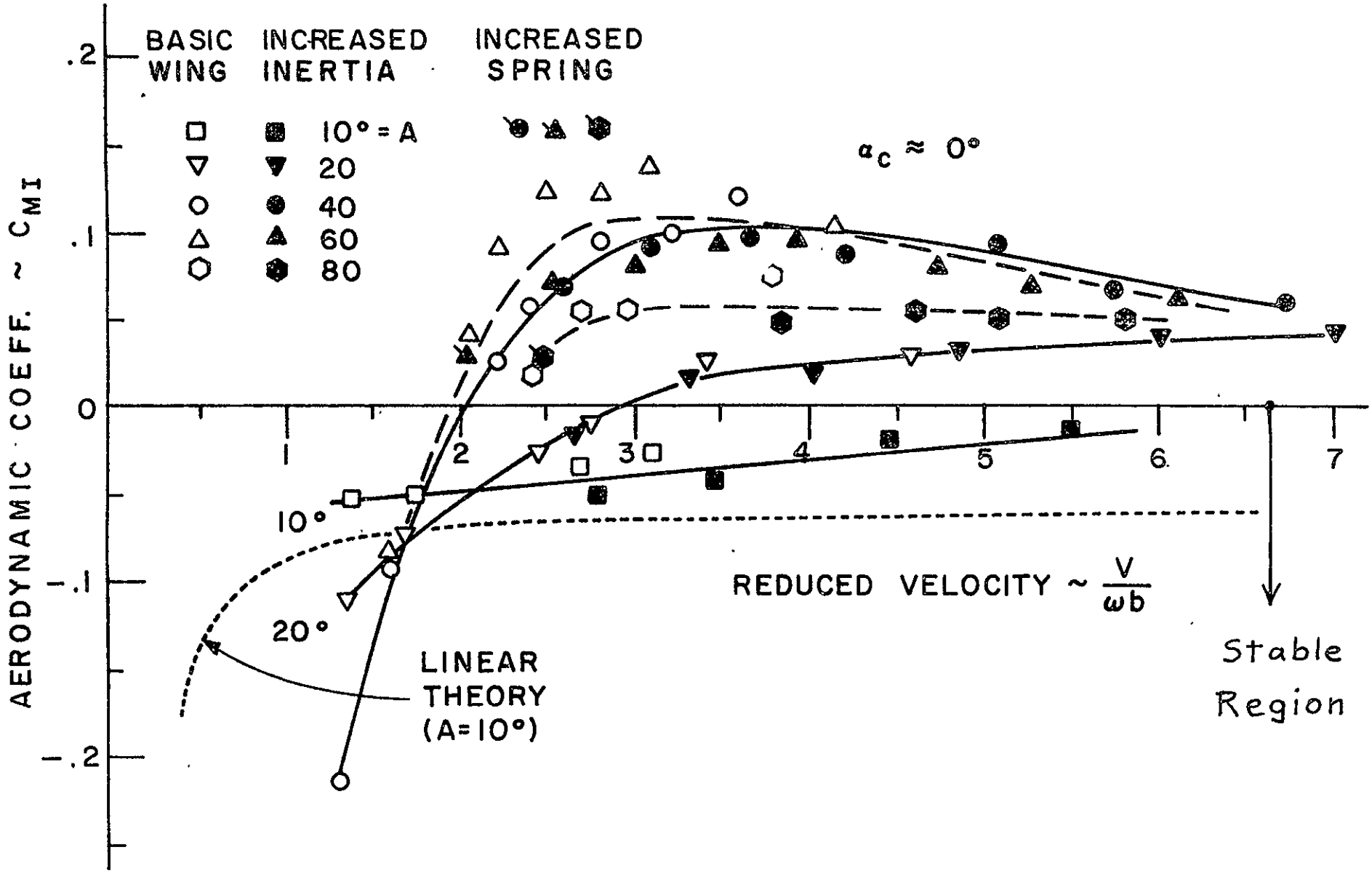

FIG. 7A EXPERIMENTAL C_{MI} CURVES ($\alpha_c \approx 0°$)

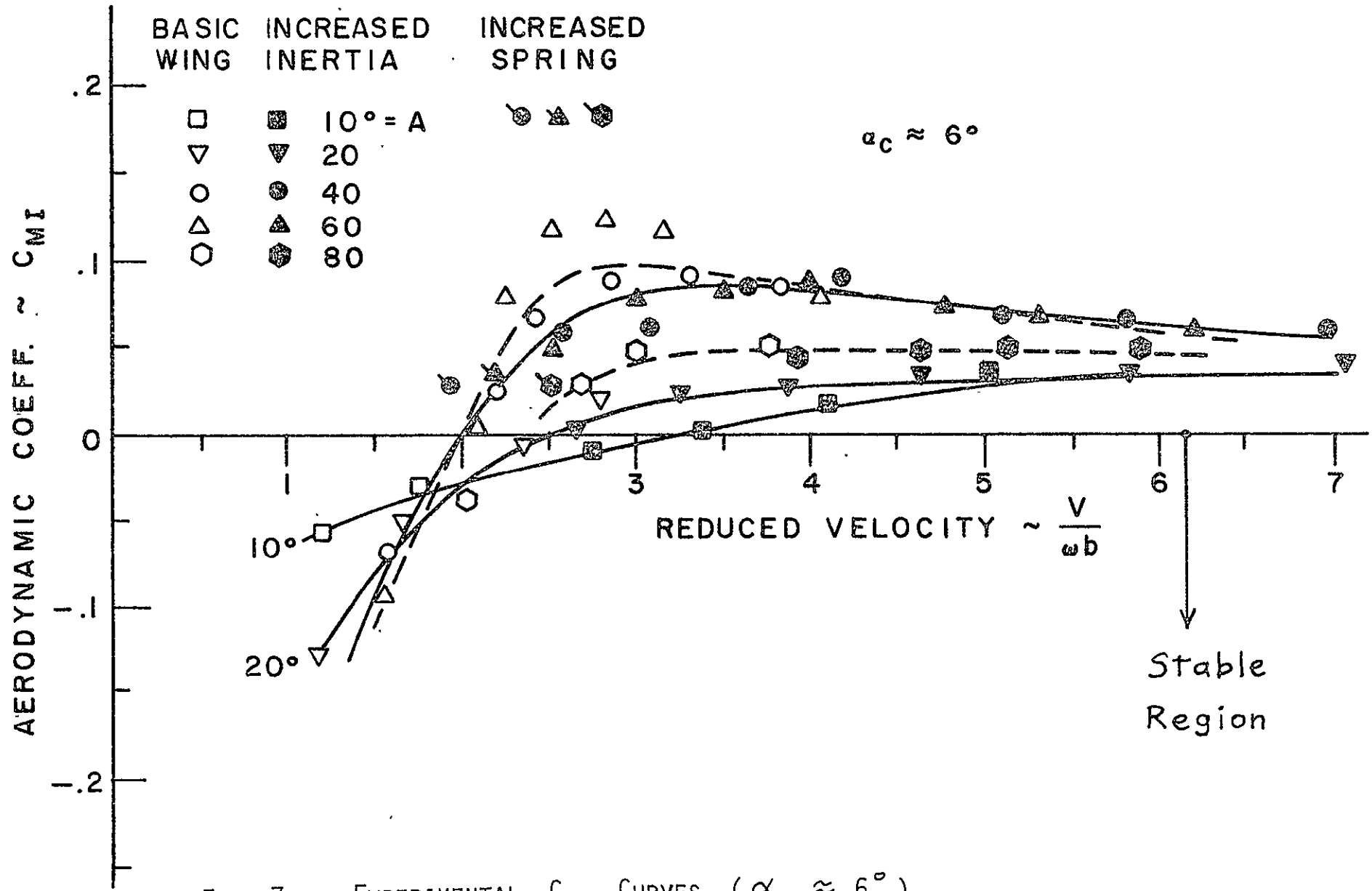

FIG. 7B EXPERIMENTAL C_{MI} CURVES ($\alpha_c \approx 6°$)

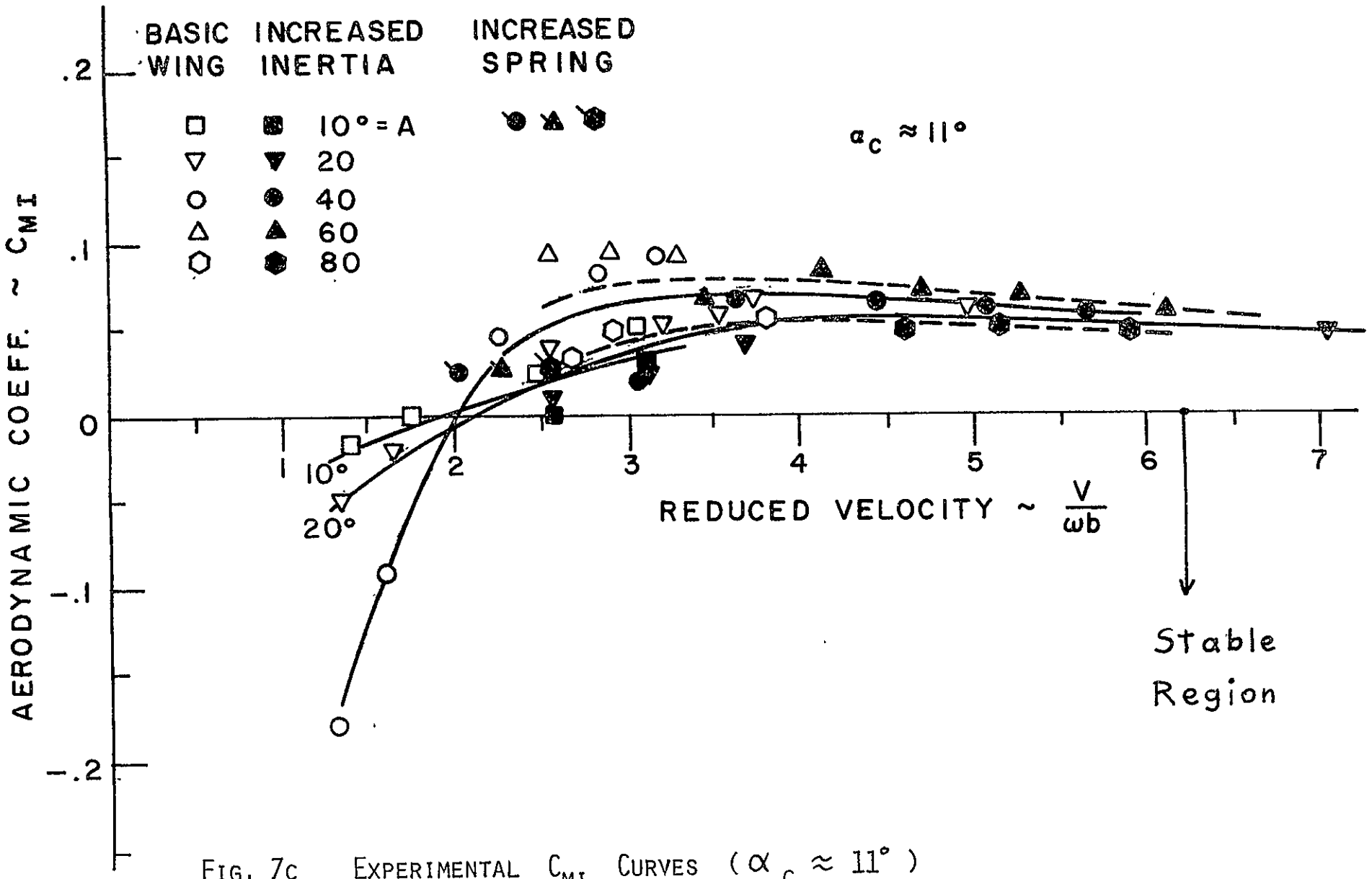

FIG. 7c EXPERIMENTAL C_{MI} CURVES ($\alpha_c \approx 11°$)

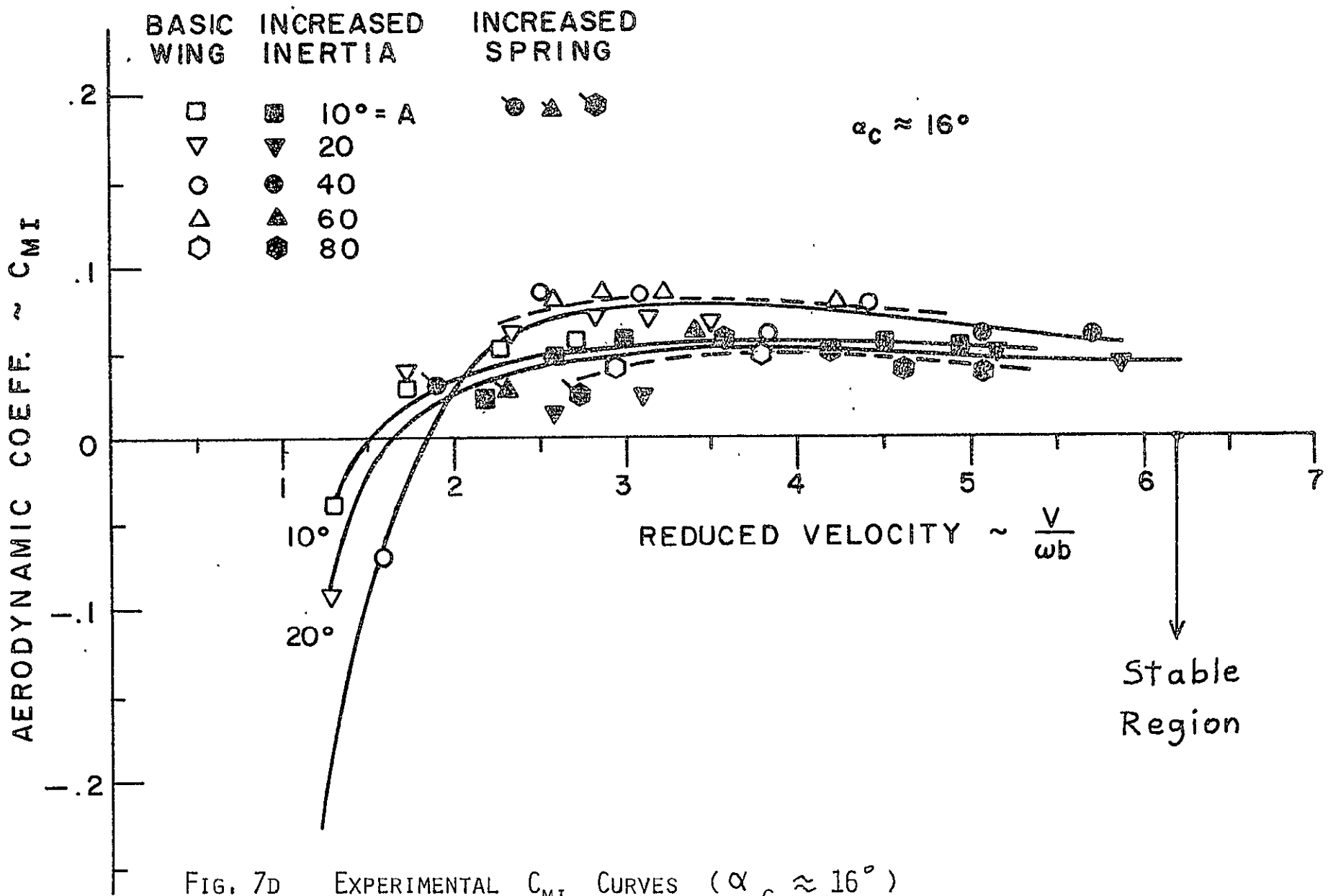

FIG. 7D EXPERIMENTAL C_{MI} CURVES ($\alpha_c \approx 16°$)

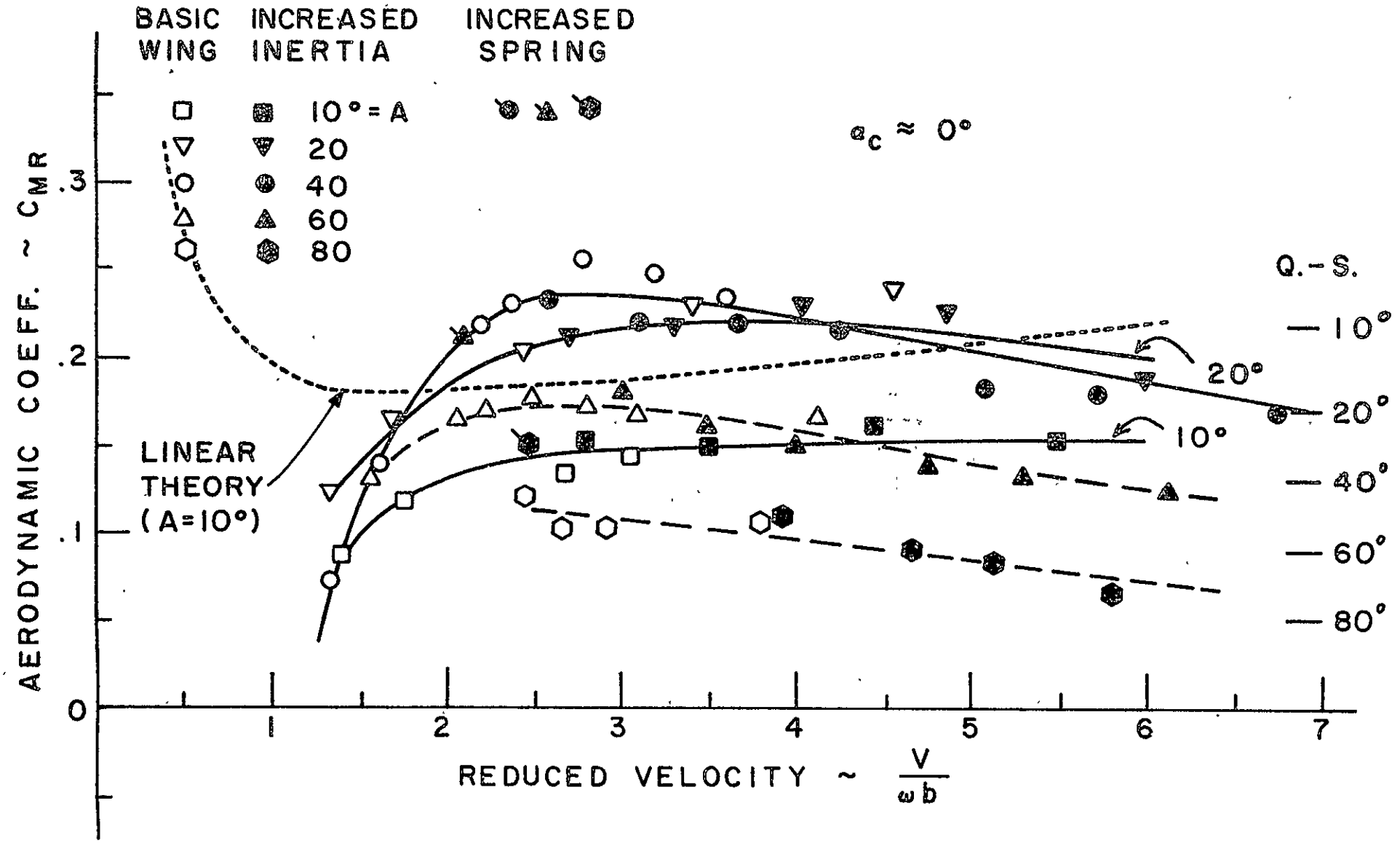

FIG. 8A EXPERIMENTAL C_{MR} CURVES ($\alpha_c \approx 0°$)

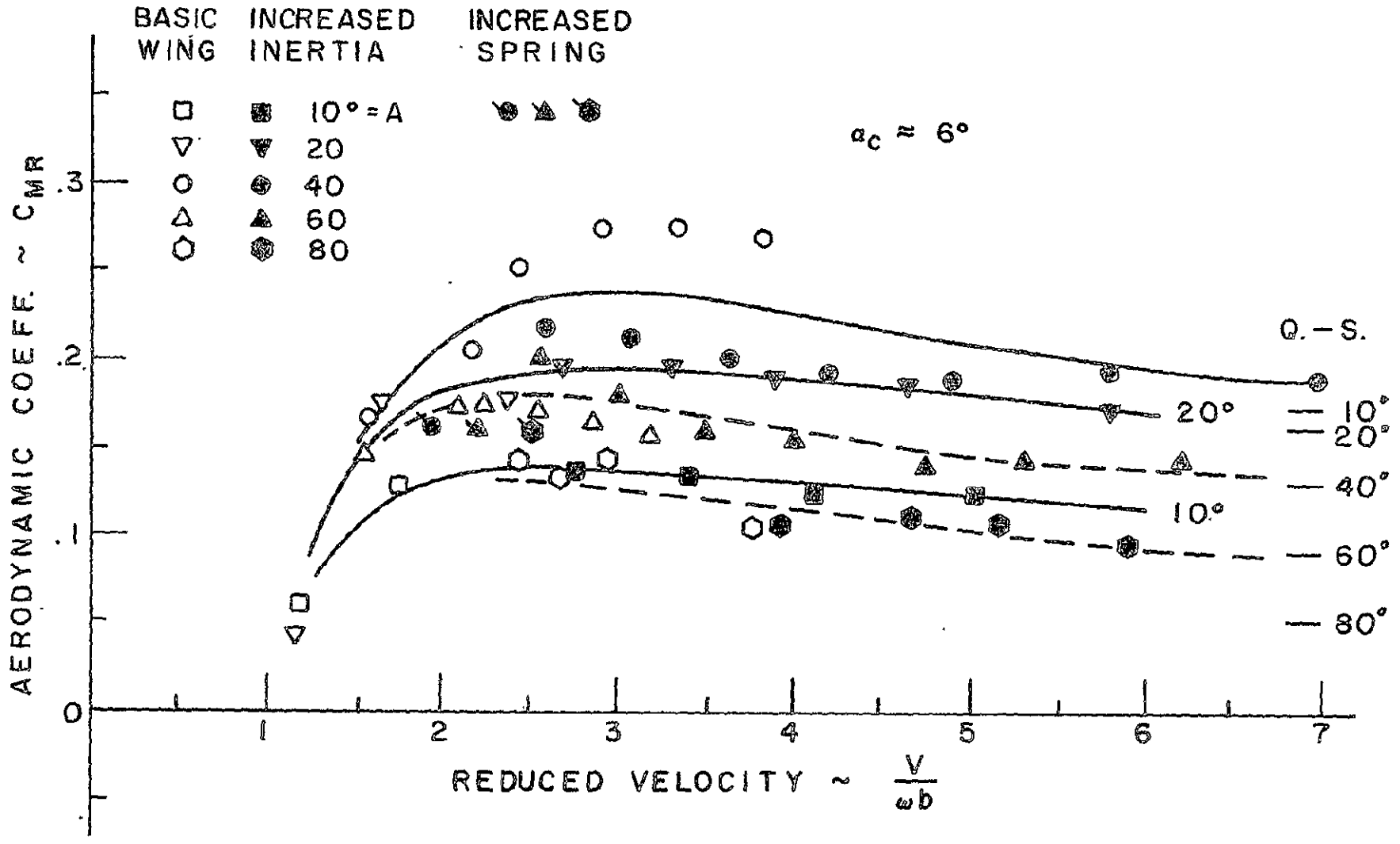

FIG. 8B EXPERIMENTAL C_{MR} CURVES ($\alpha_c \approx 6°$)

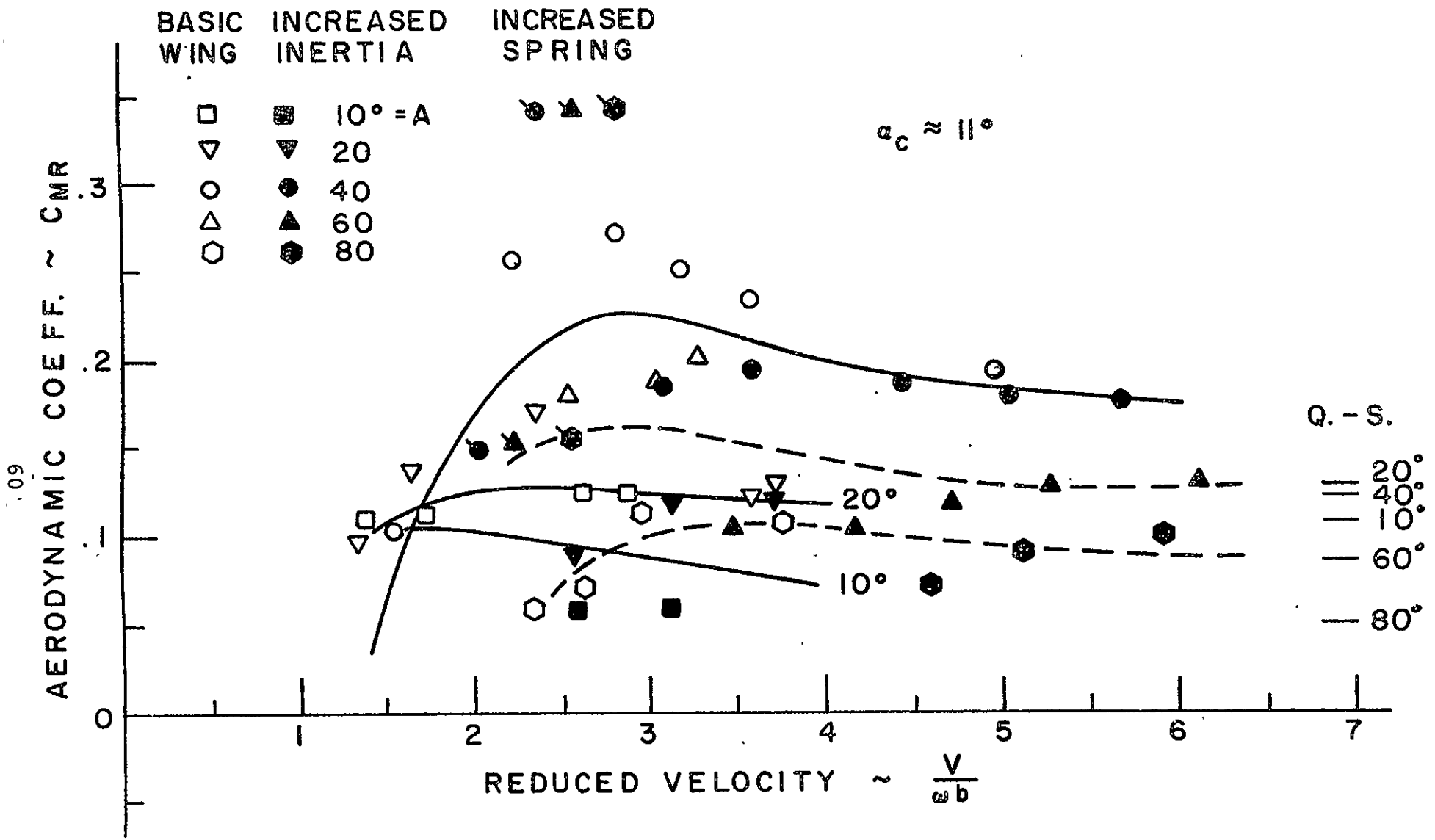

FIG. 8C EXPERIMENTAL C_{MR} CURVES ($\alpha_c \approx 11°$)

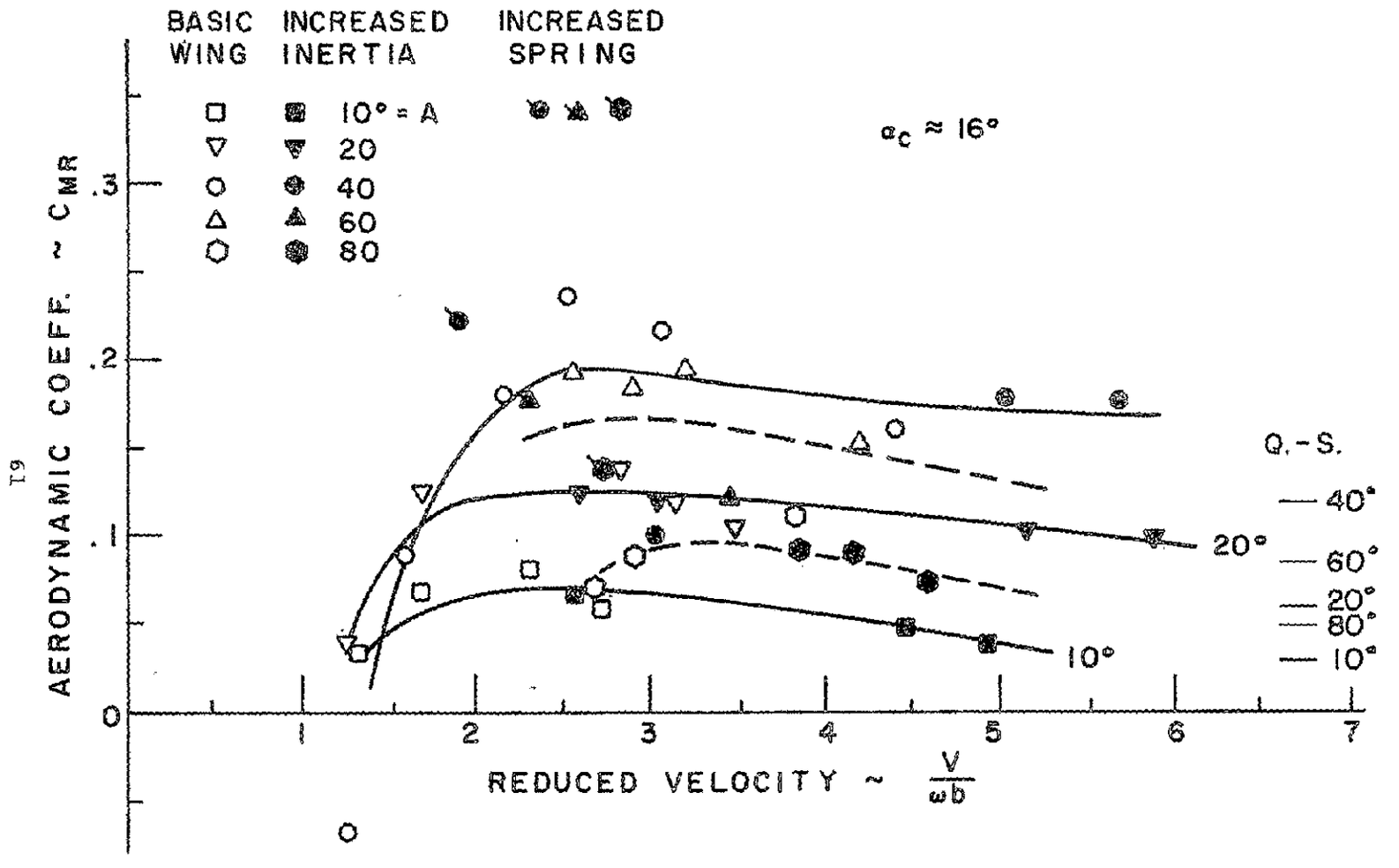

FIG. 8D EXPERIMENTAL C_{MR} CURVES ($\alpha_c \approx 16°$)

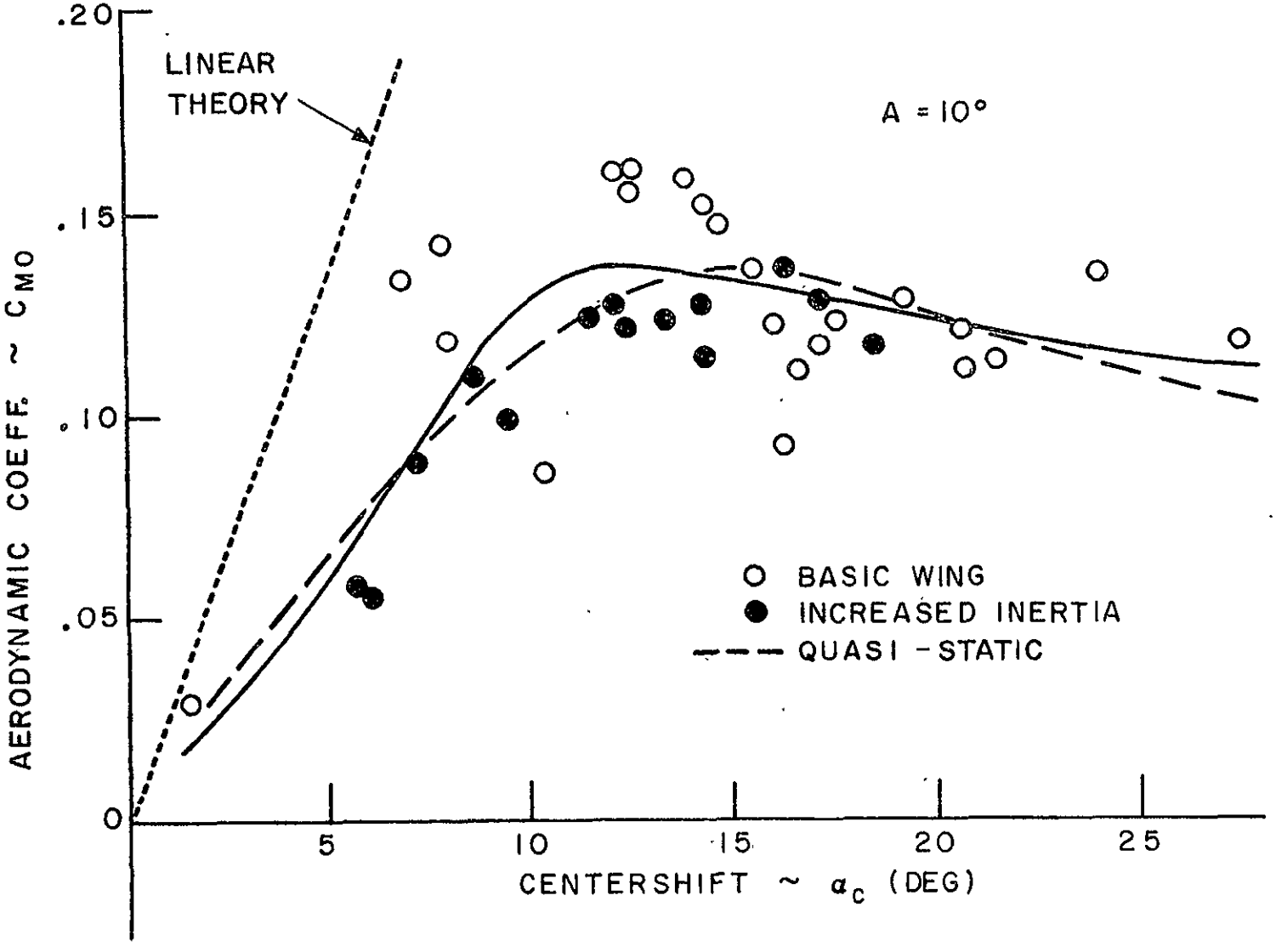

FIG. 9A EXPERIMENTAL C_{MO} CURVES (A = 10°)

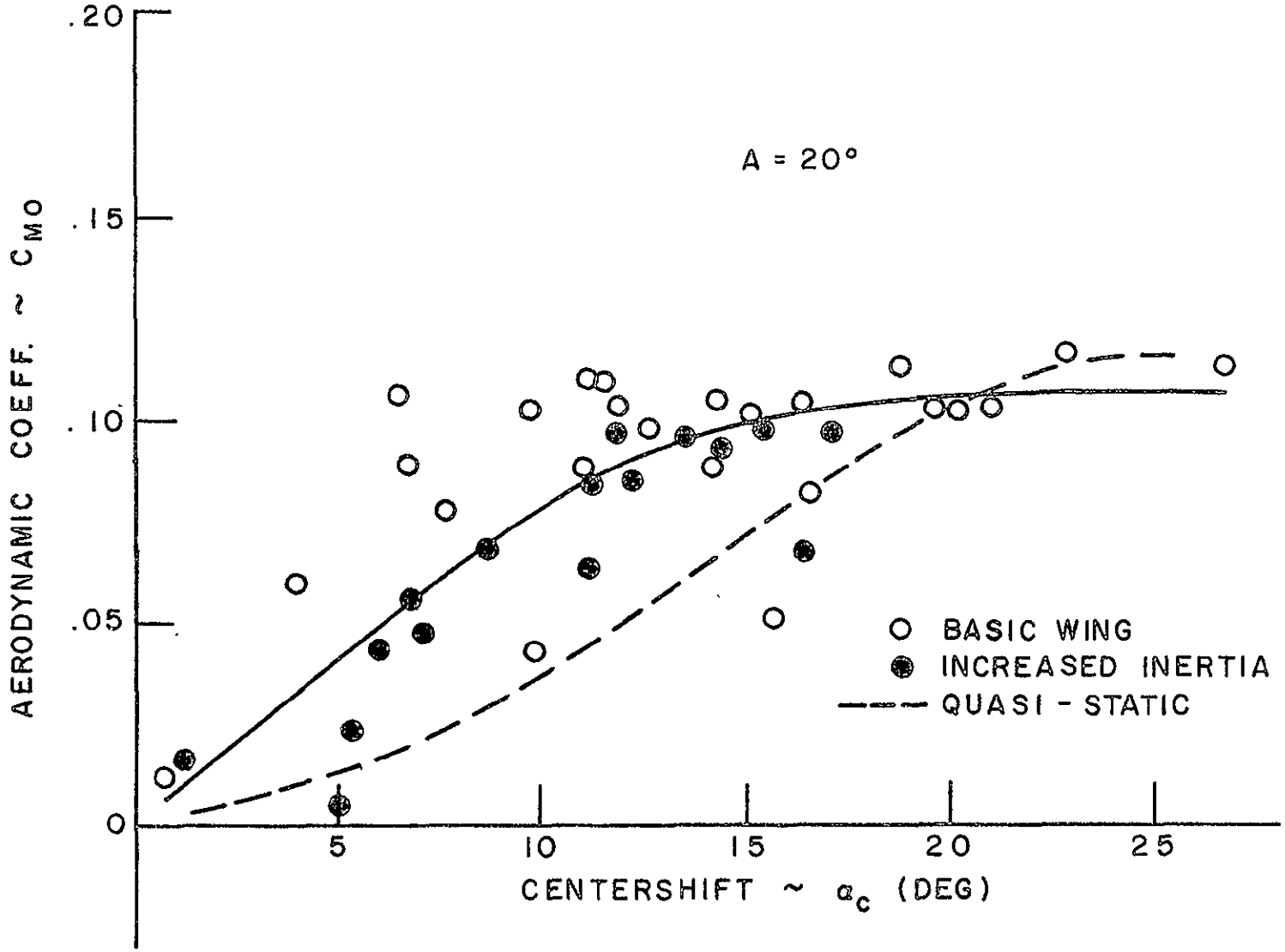

FIG. 9B EXPERIMENTAL C_{MO} CURVES (A = 20°)

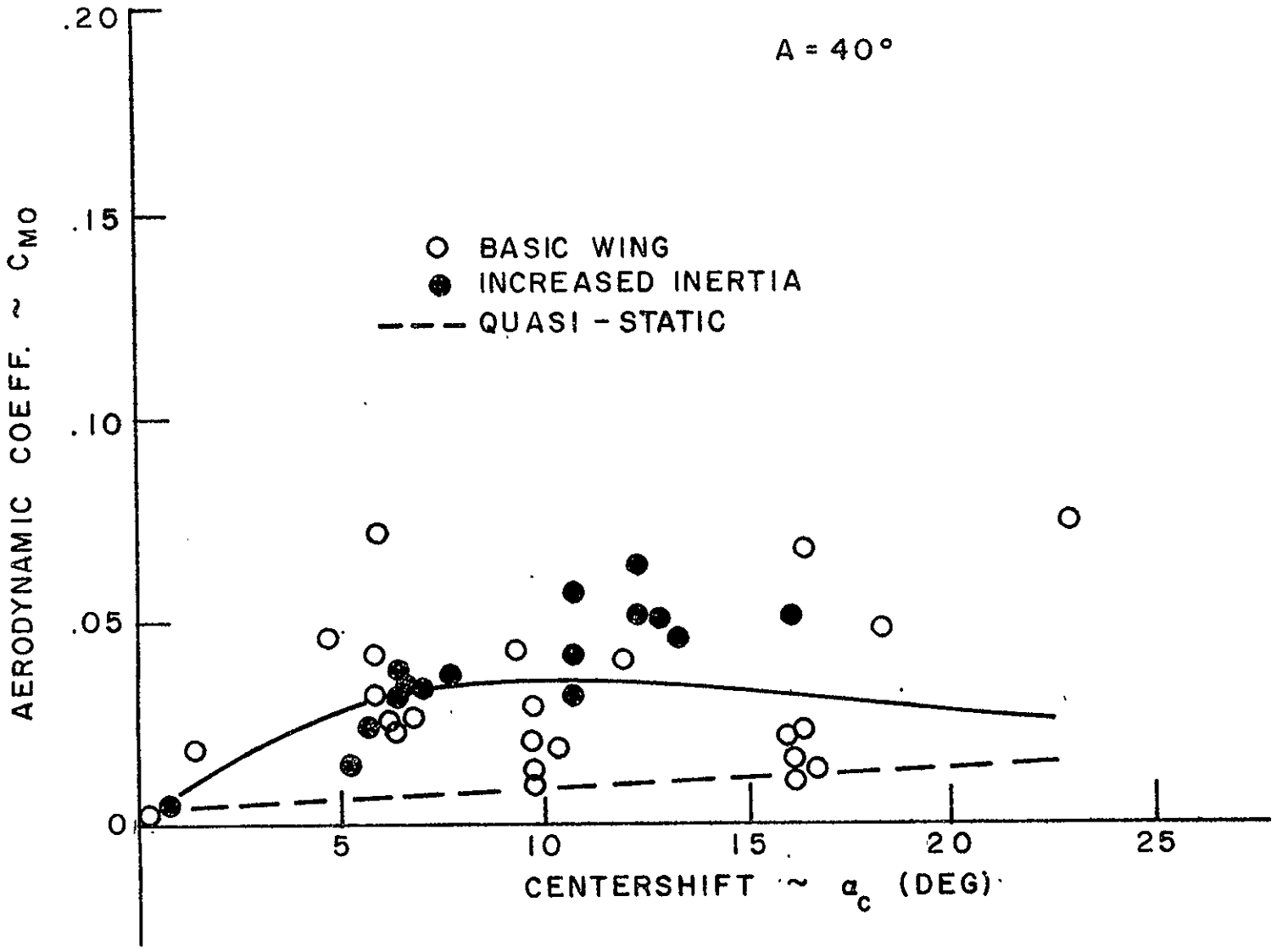

FIG. 9C EXPERIMENTAL C_{MO} CURVES (A = 40°)

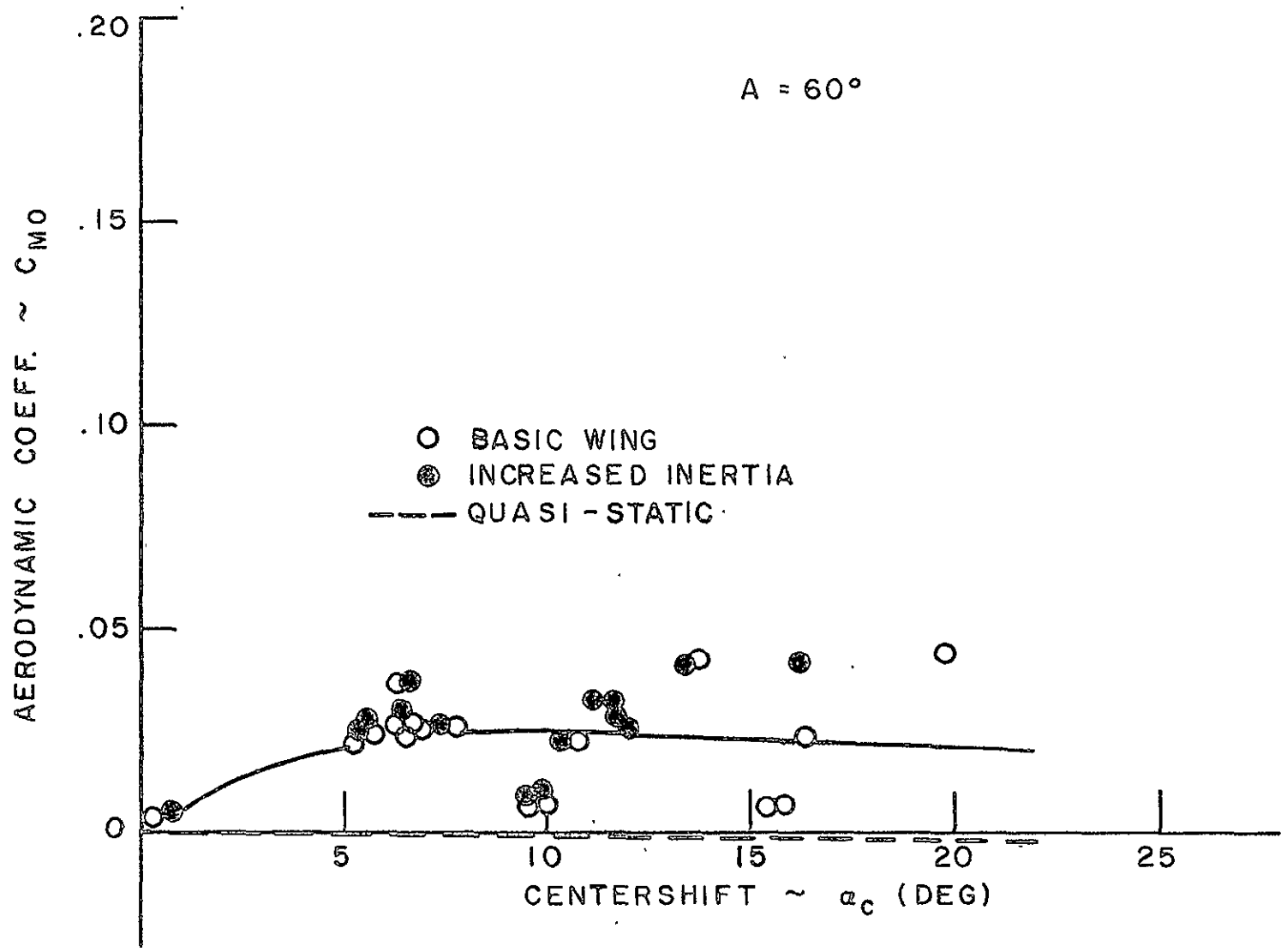

FIG. 9D EXPERIMENTAL C_{MO} CURVES (A = 60°)

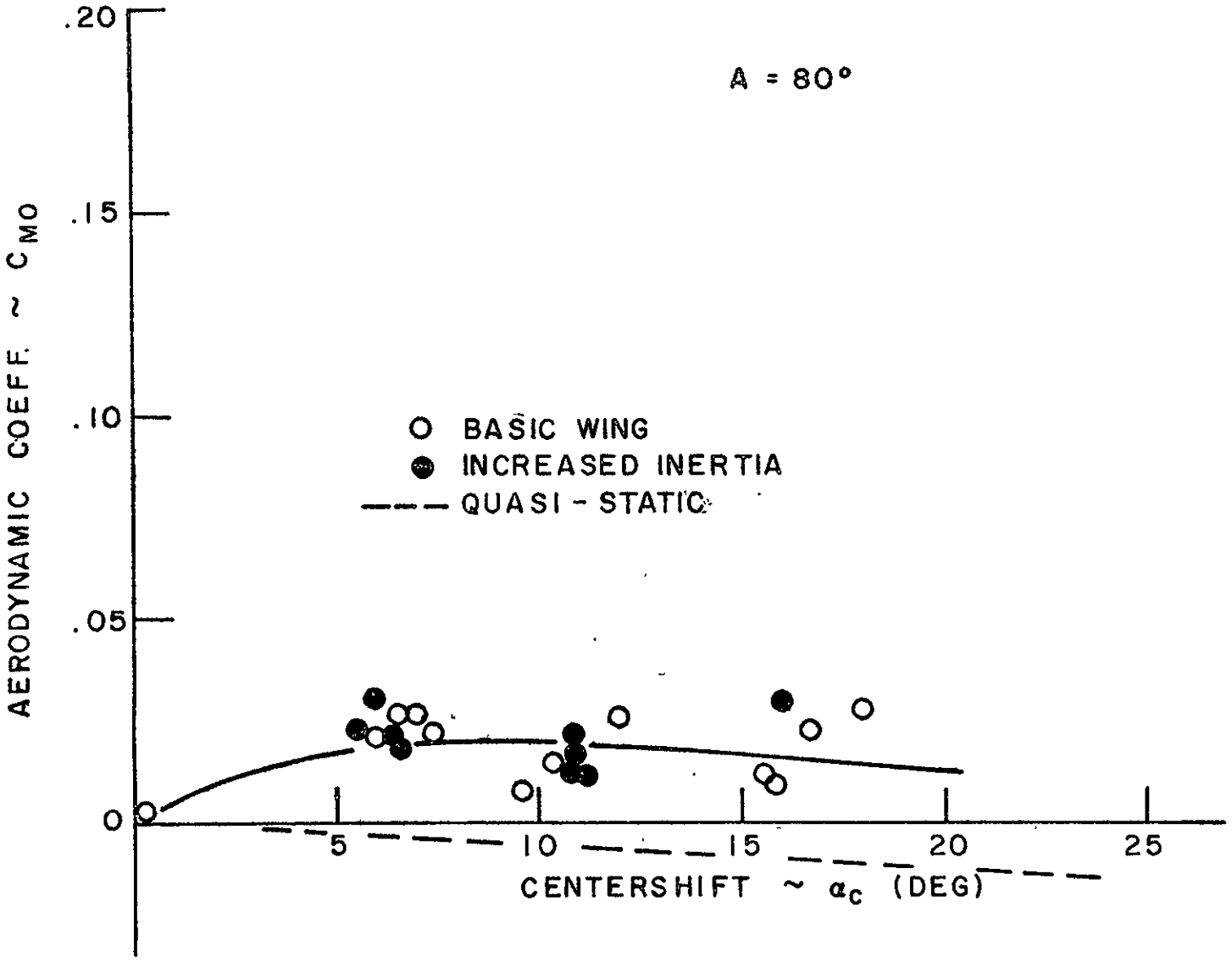

FIG. 9E EXPERIMENTAL C_{MO} CURVES (A = 80°)

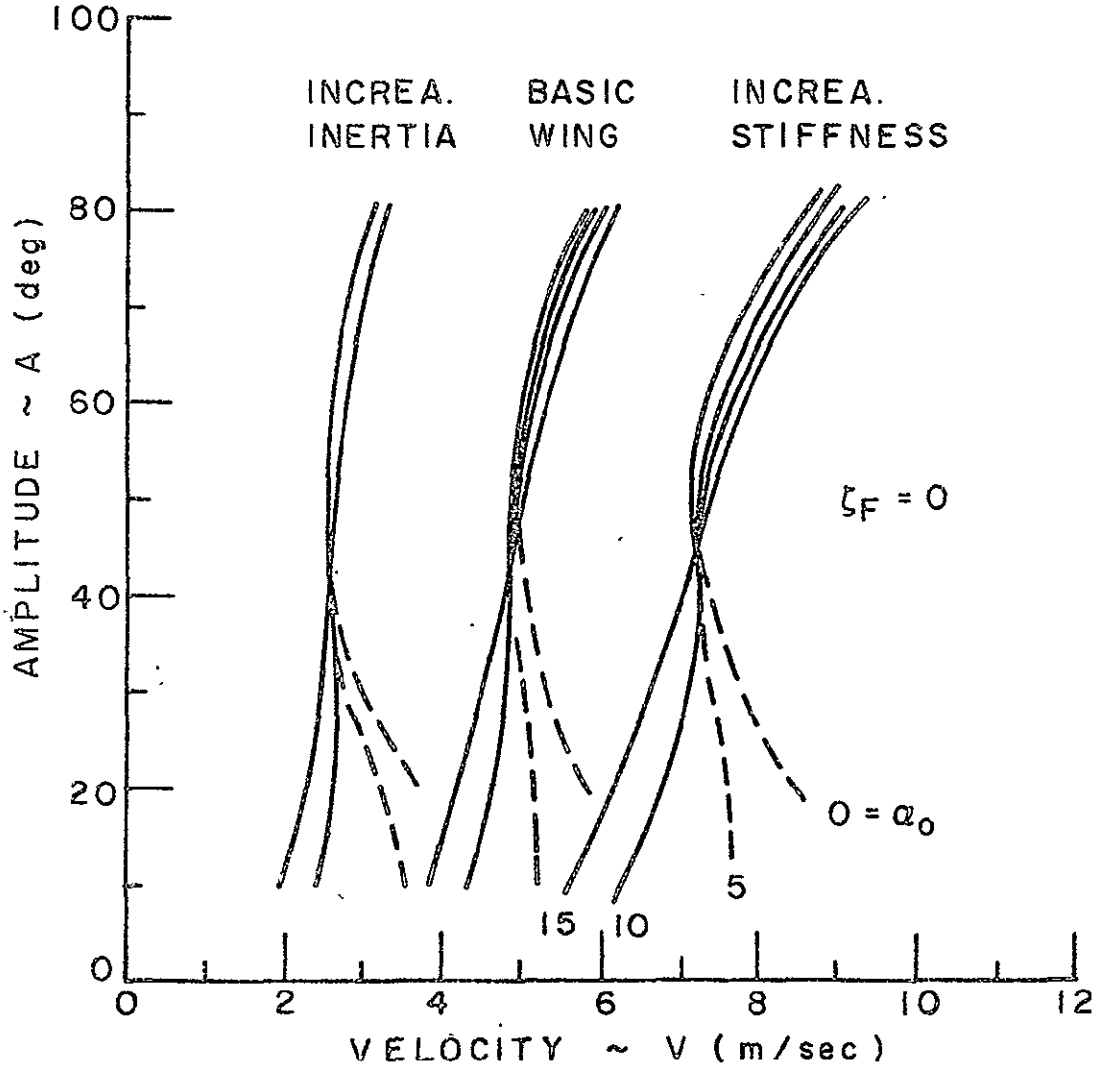

FIG. 10 CALCULATED FLUTTER AMPLITUDES FOR NO FRICTION

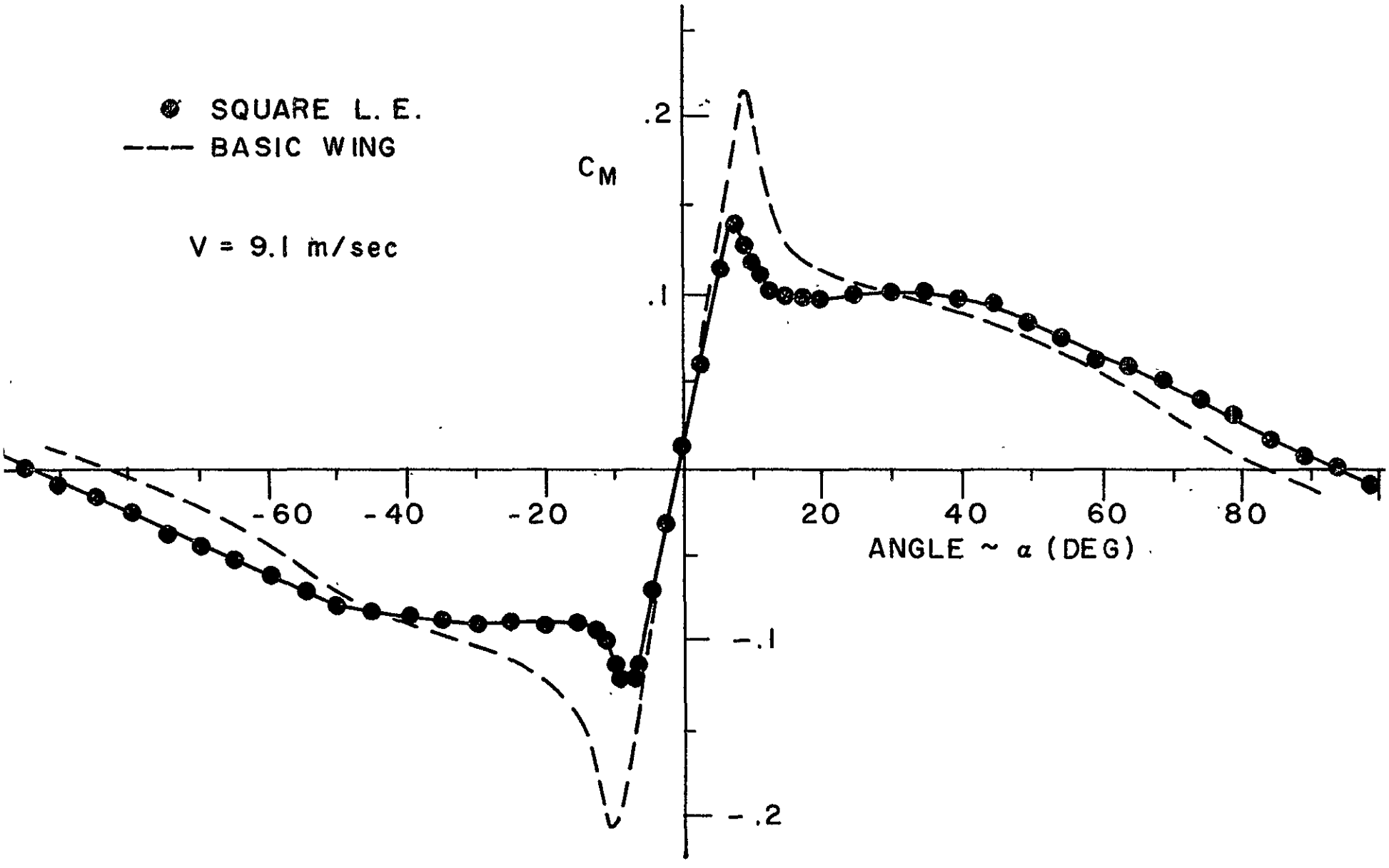

FIG. 11 STATIC MOMENT (SQUARE L.E. WING)

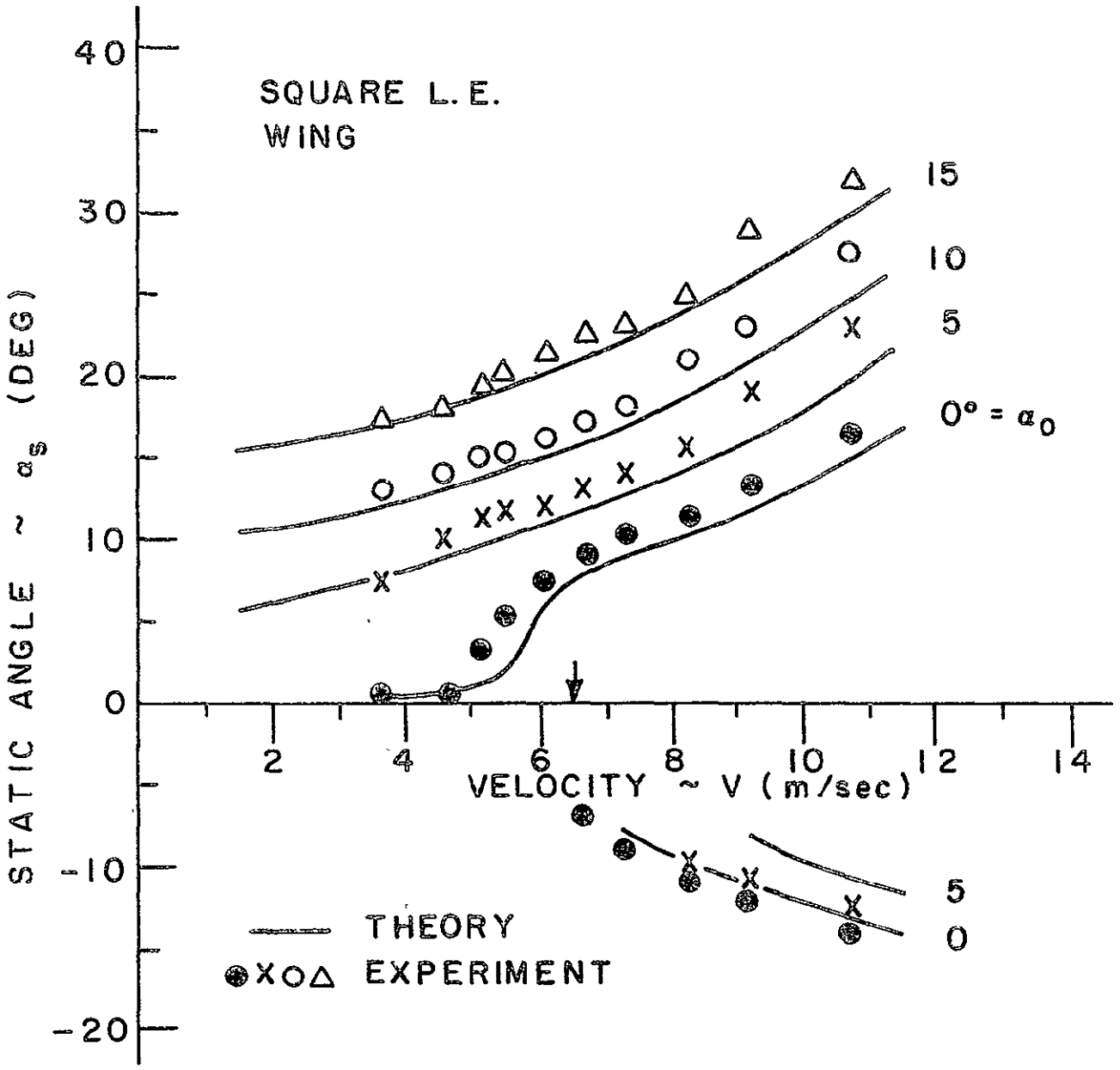

FIG. 12 STATIC DIVERGENCE (SQUARE L.E. WING)

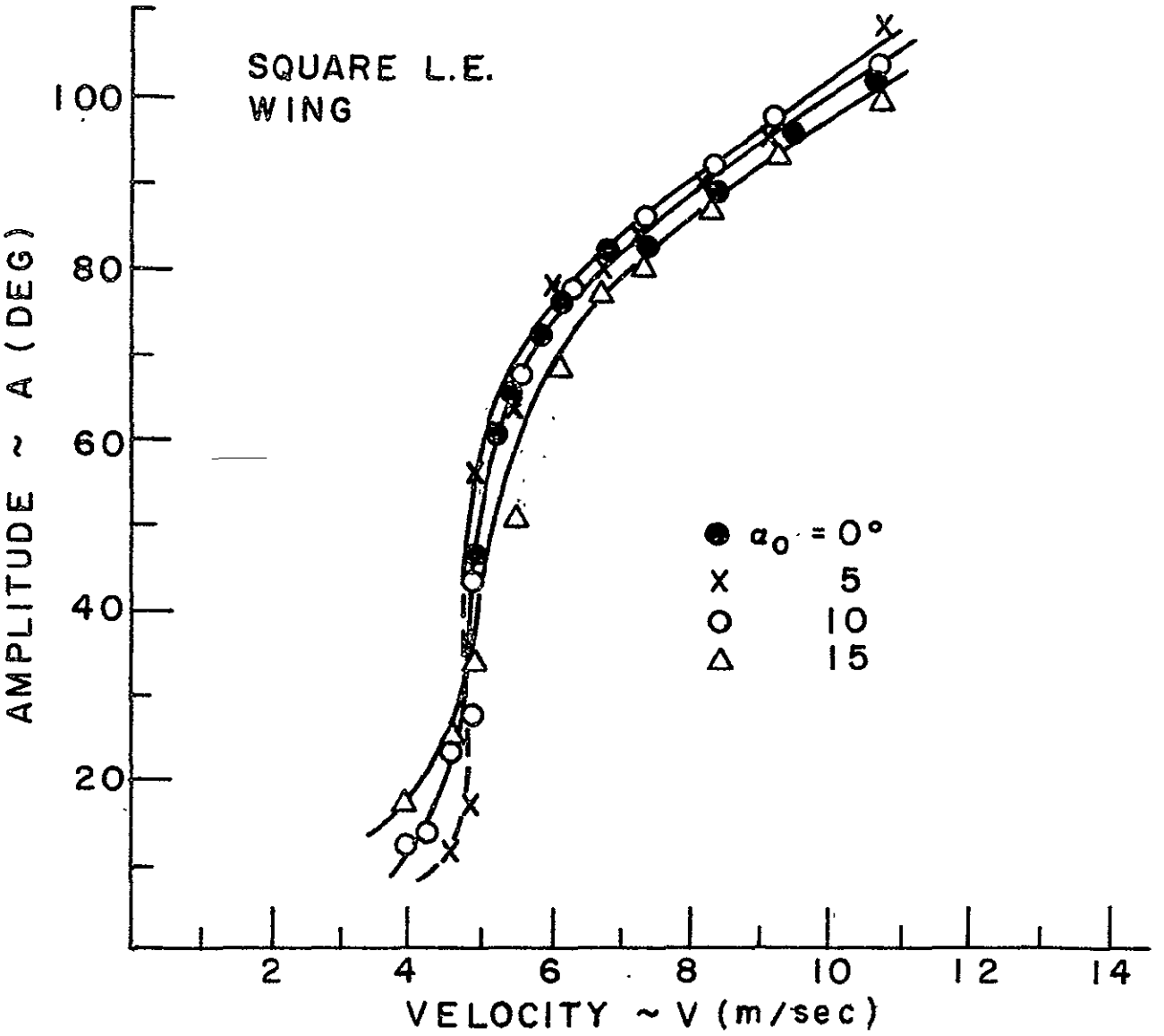

FIG. 13A FLUTTER AMPLITUDES (SQUARE L.E. WING)

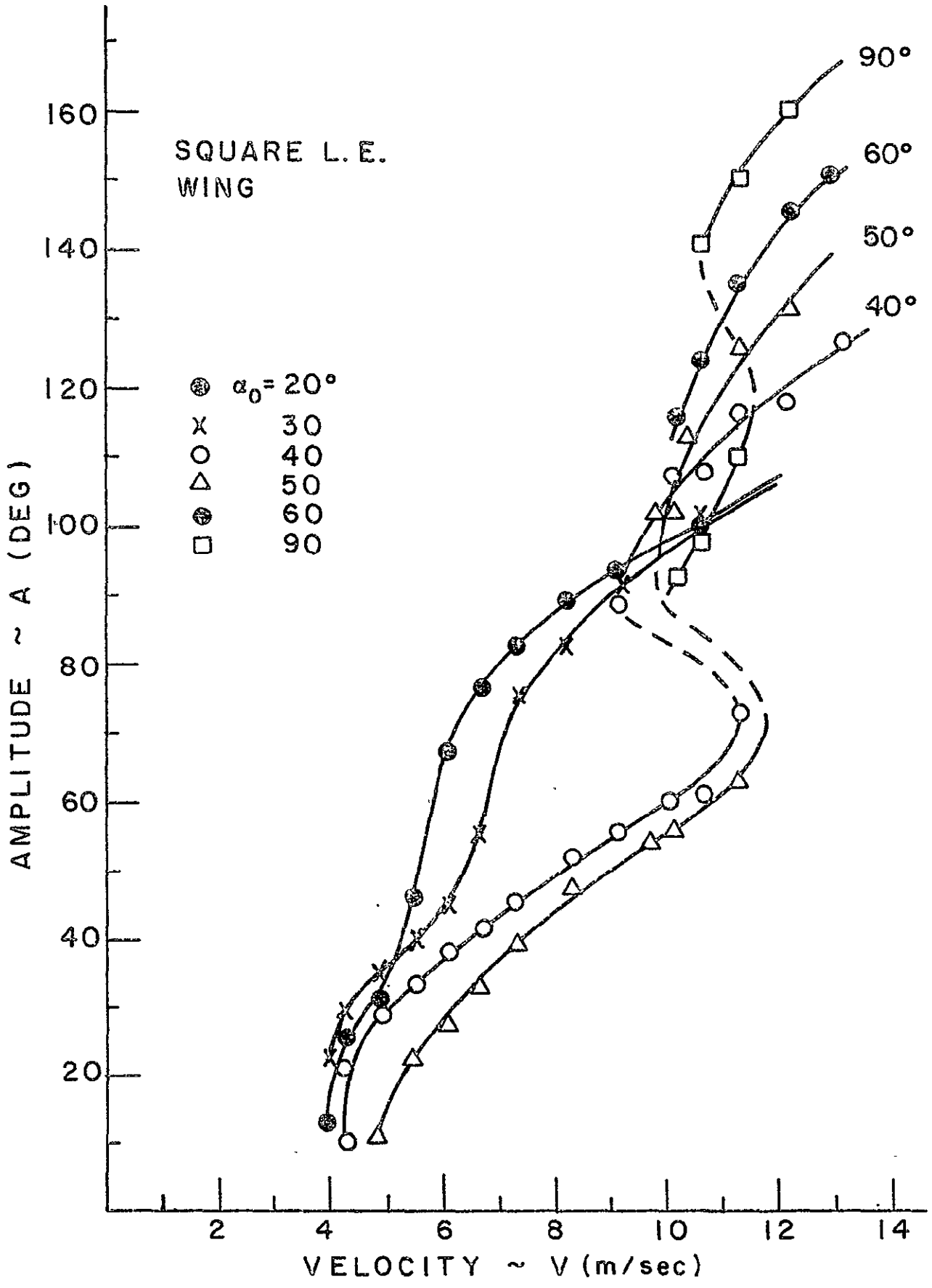

FIG. 13B FLUTTER AMPLITUDES (SQUARE L.E. WING)

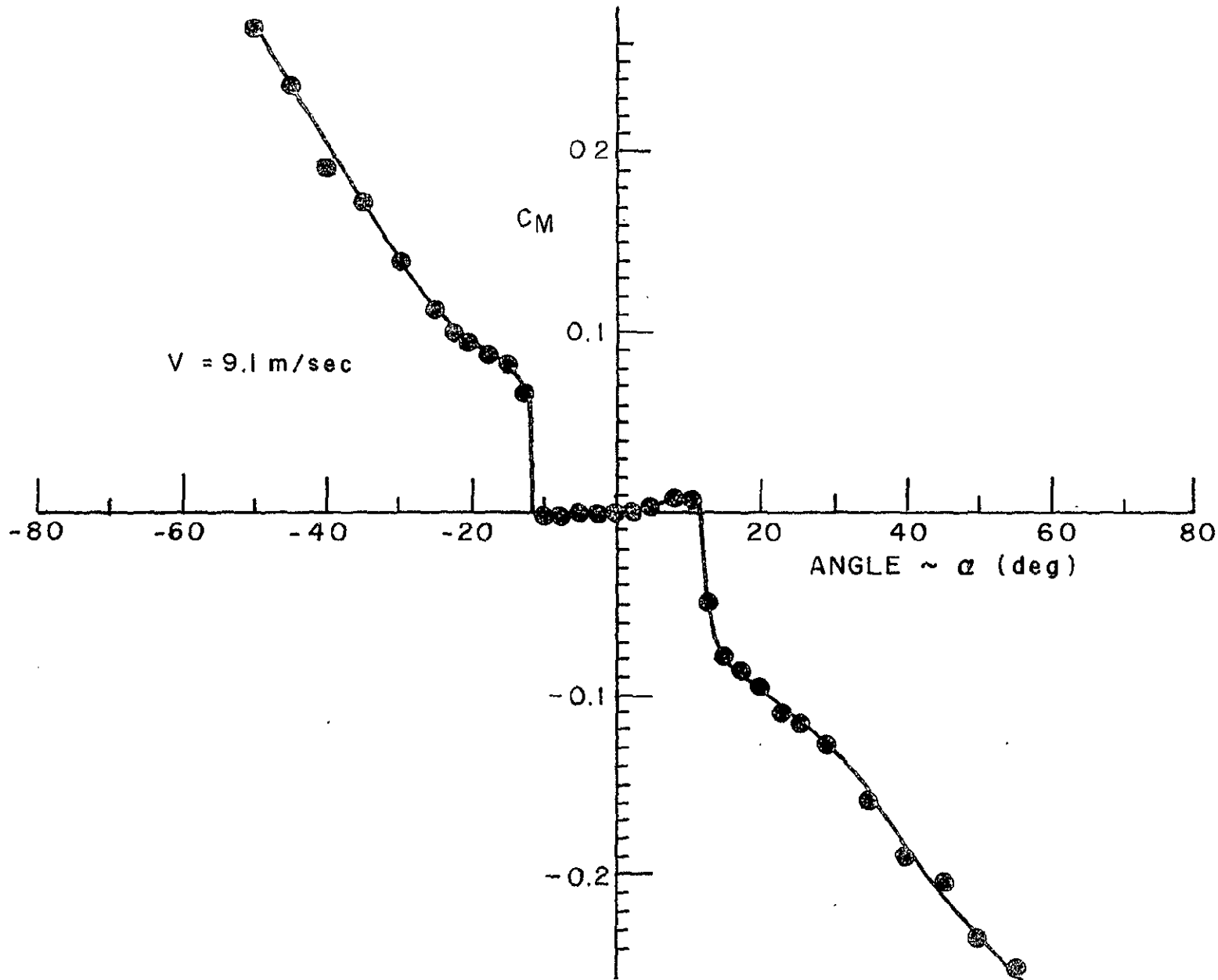

FIG. 17 STATIC MOMENT FOR BENDING-TORSION WING SECTION

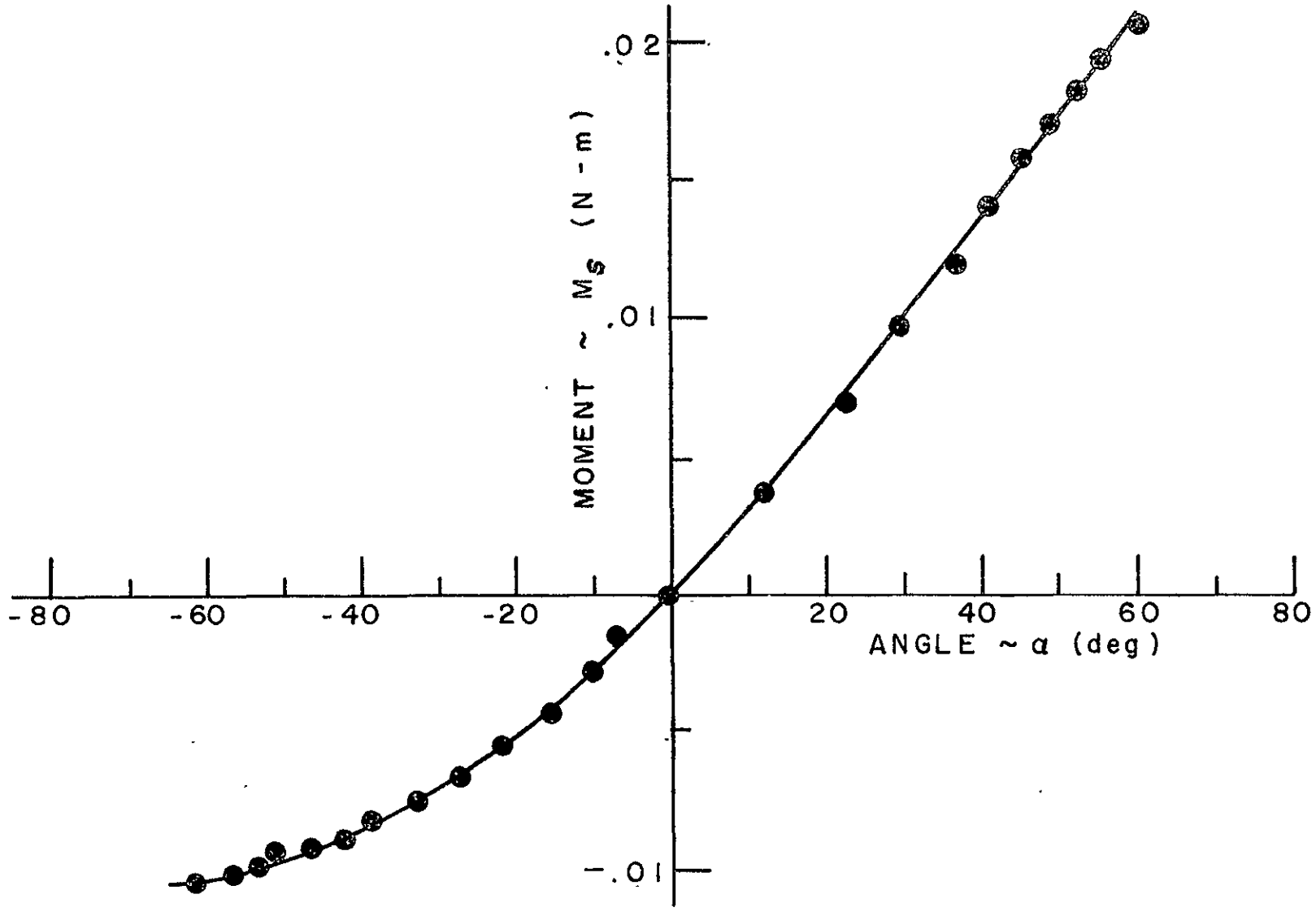

FIG. 18 SPRING MOMENT VS. WING ANGLE OF ATTACK

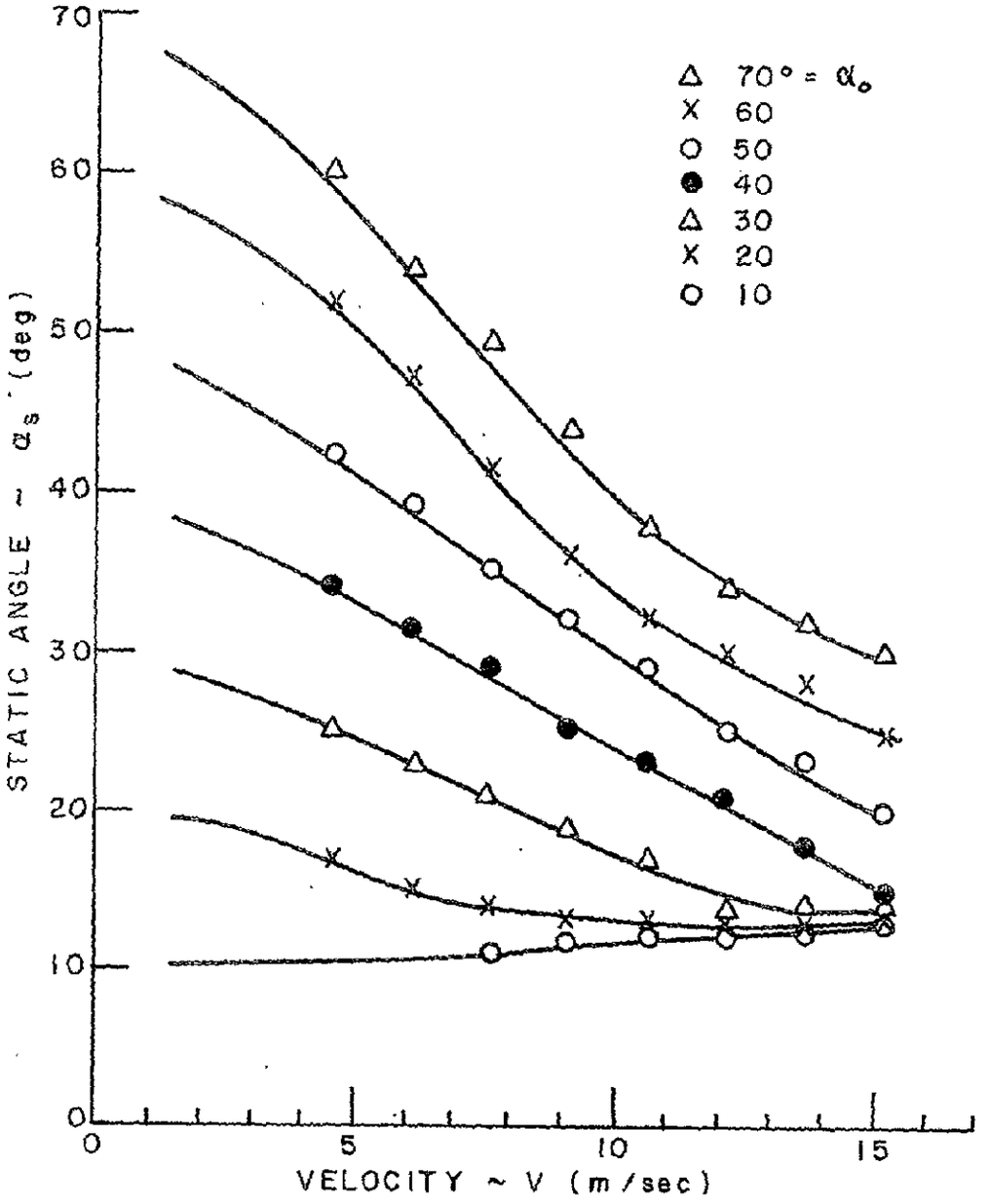

FIG. 19 STATIC EQUILIBRIUM FOR BENDING-TORSION WING SECTION

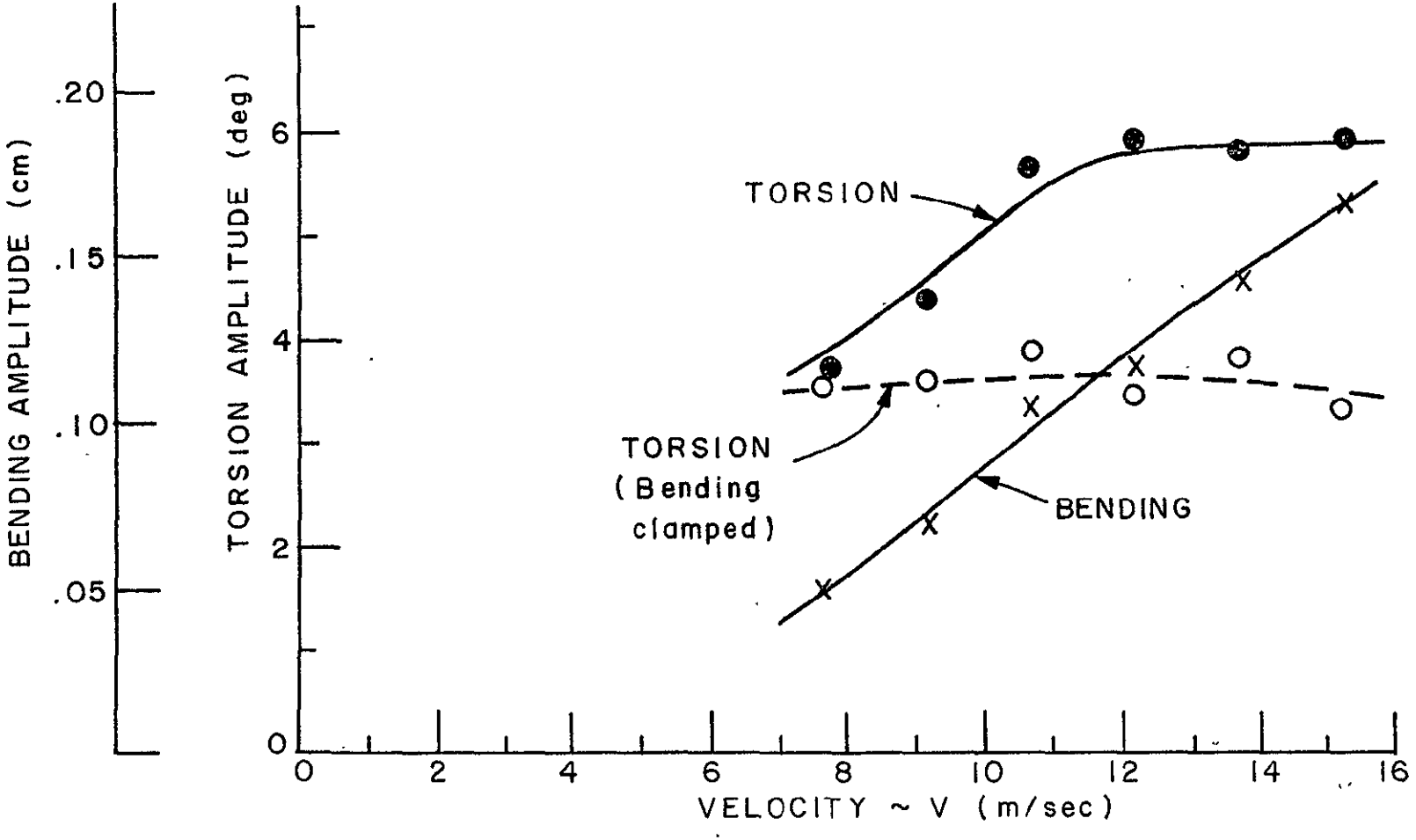

FIG. 21c FLUTTER AMPLITUDES FOR SMALL STALL FLUTTER

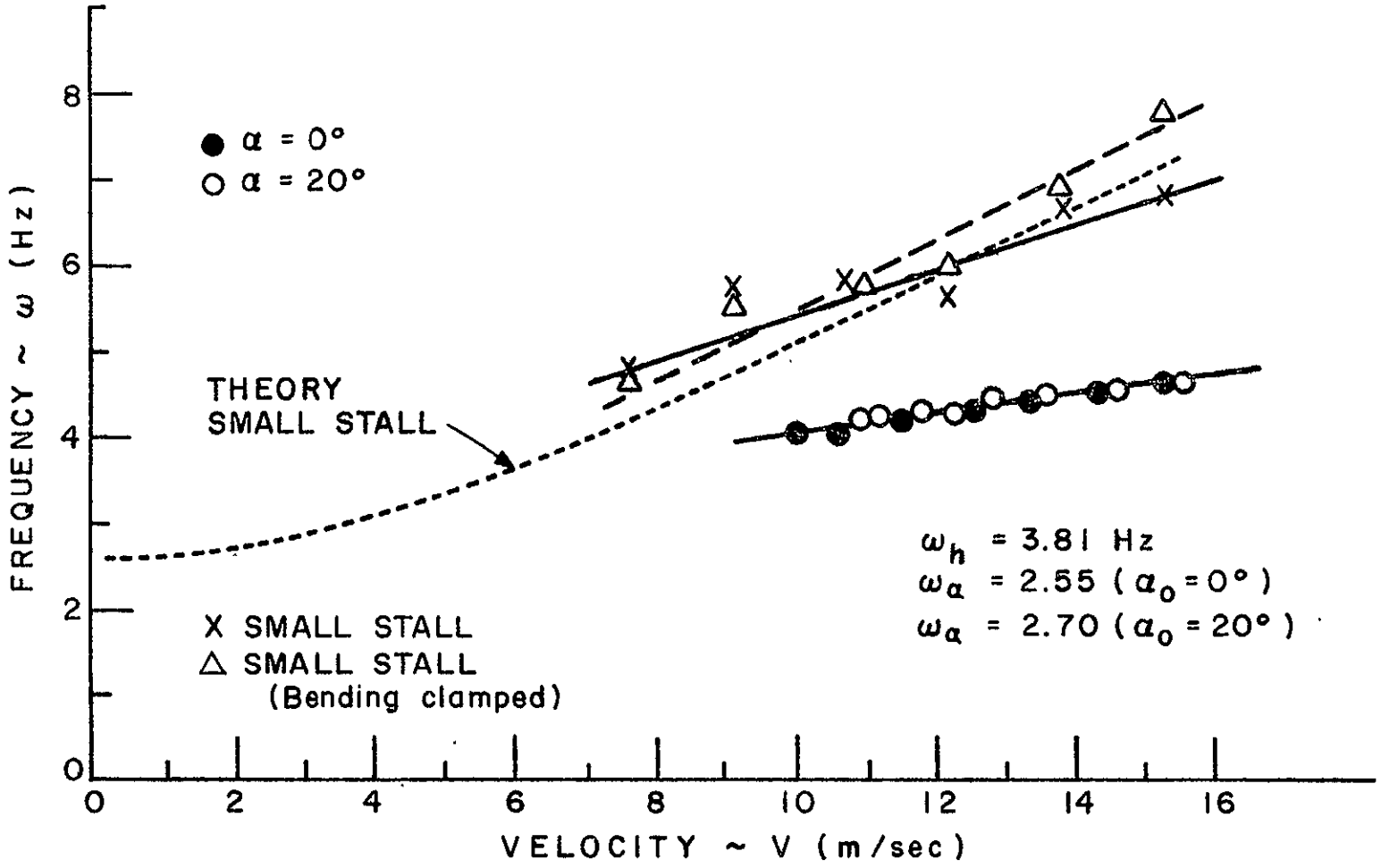

FIG. 22 FLUTTER FREQUENCIES FOR BENDING-TORSION WING

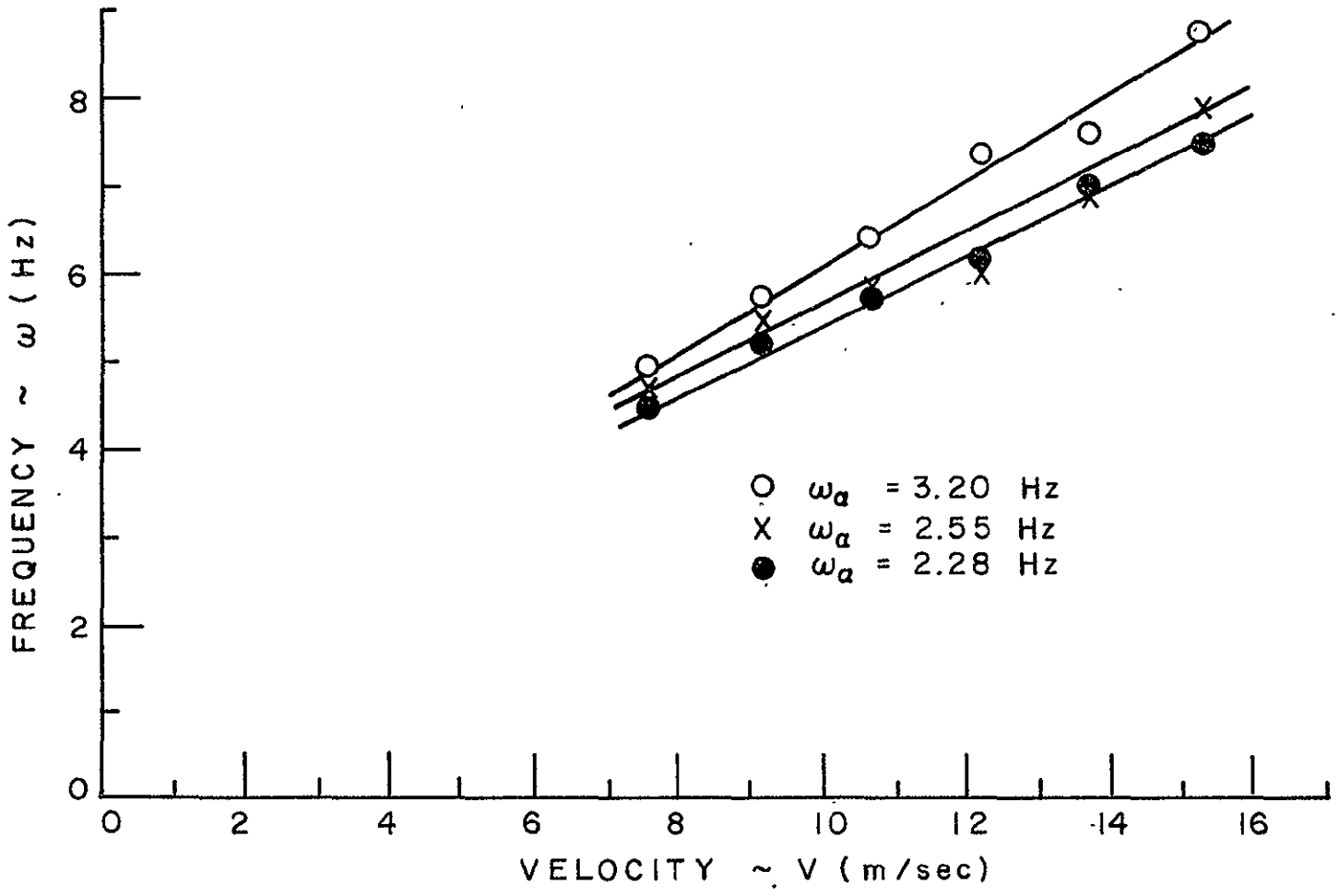

FIG. 23 FREQUENCIES FOR SMALL STALL FLUTTER (PURE TORSION)

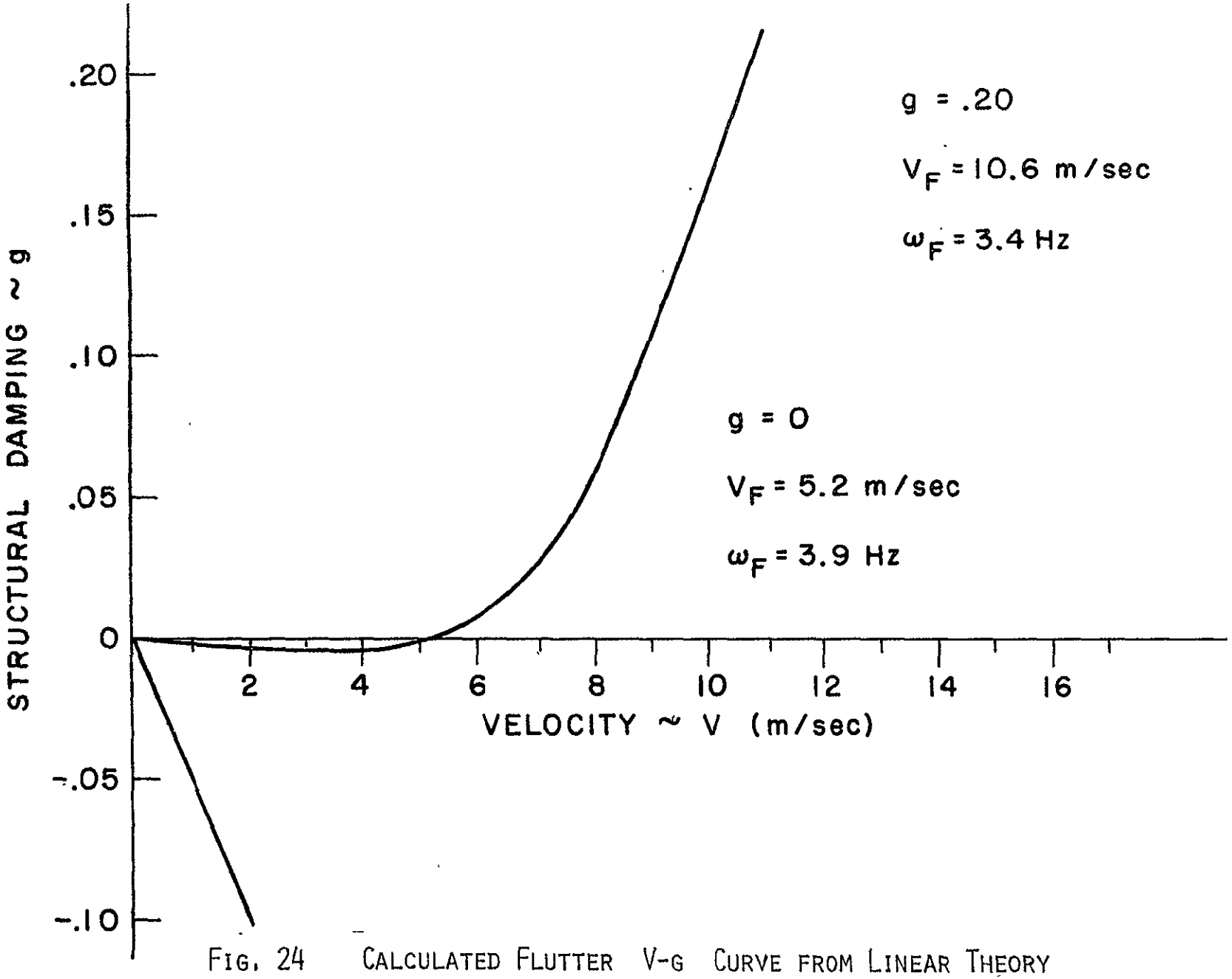

FIG. 24 CALCULATED FLUTTER V-G CURVE FROM LINEAR THEORY